Tectonophysics 654 (2015) 30–55

Contents lists available at ScienceDirect

Tectonophysics

journal homepage: www.elsevier.com/locate/tecto

Post break-up tectonic inversion across the southwestern cape of South Africa: New insights from apatite and zircon fission track thermochronometry

Mark Wildman [a,*], Roderick Brown [a], Ron Watkins [b], Andrew Carter [c], Andrew Gleadow [d], Michael Summerfield [e]

[a] School of Geographical and Earth Sciences, College of Science and Engineering, University of Glasgow, Gregory Building, Glasgow, G12 8QQ Scotland, United Kingdom
[b] Faculty of Science and Engineering, Western Australian School of Mines, Department of Applied Geology, Curtin University of Technology, GPO Box U1987, Perth, WA 6845, Australia
[c] Department of Earth and Planetary Sciences, Birkbeck, University of London, Malet Street, WC1E 7HX, United Kingdom
[d] School of Earth Sciences, University of Melbourne, Melbourne 3010, Australia
[e] Institute of Geography, University of Edinburgh, Drummond Street, Edinburgh, EH8 9XP Scotland, United Kingdom

ARTICLE INFO

Article history:
Received 23 July 2014
Received in revised form 6 March 2015
Accepted 29 April 2015
Available online 10 May 2015

Keywords:
Fission track
Continental margin
Thermal history modelling
Southwestern Africa
Thermochronology

ABSTRACT

The south-west African margin is regarded as an example of a passive continental margin formed by continental rifting following a phase of lithospheric extension and thinning. Recent attention focused on this margin has included theoretical modelling studies of rift processes, plate kinematic studies of the opening geometry and timing, and empirical studies focused on documenting the crustal structure and offshore sedimentary record. Here, we examine the onshore geomorphic and tectonic response to rifting and breakup, with a specific focus on the SW Cape of South Africa. We present 75 new apatite and 8 new zircon fission track analyses from outcrop samples and onshore borehole profiles along the western margin of South Africa. The data are used to derive robust thermal histories that record two discrete phases of accelerated erosional cooling during the Early Cretaceous (150–130 Ma) and Late Cretaceous (100–80 Ma), respectively. Both periods of enhanced erosion are regional in extent, involved km-scale erosion, and extend well inland of the current escarpment zone, albeit with spatially variable intensity and style. The Late Cretaceous episode is also expressed more locally by tectonic reactivation and inversion of major faults causing km-scale differential displacement and erosion. The new AFT data do not exclude the possibility of modest surface uplift occurring during the Cenozoic, but they restrict the depth of regional Cenozoic erosion on the western margin to less than c. 1 km. The inferred pattern and chronology of erosion onshore is consistent with the key features and sediment accumulation patterns within the offshore Orange and Bredasdorp basins. It is suggested that the Late Cretaceous event was triggered by a combination of regional dynamic uplift augmented along the western margin and in the SW Cape by local tectonic forces arising from dextral displacement of the Falkland Plateau along the Falkland–Agulhas Fracture Zone.

1. Introduction

The widespread occurrence of prominent coast-parallel escarpments along high-elevation passive margins is a strong indication that significant relief is generated along the edge of separating continental plates as a consequence of rifting with examples being southern Africa, western India and southeastern Australia (e.g., Matmon et al., 2002; Ollier, 1985; Summerfield, 2000). However, despite numerous studies focusing on the geodynamic and geomorphic processes involved during continental rifting (e.g., Braun and Beaumont, 1989; Brune et al., 2014; Gilchrist and Summerfield, 1991; Huismans and Beaumont, 2011; Japsen et al., 2006; Kooi and Beaumont, 1994; Ollier, 1985; van der Beek and Braun, 1998), the precise nature of the relationship between rifting processes and the mechanisms responsible for creating and maintaining topography is not fully understood and remains controversial (e.g., Blenkinsop and Moore, 2013; Green et al., 2013; Japsen et al., 2006; Rouby et al., 2013).

The extent to which tectonic and geomorphic responses are transmitted away from the rift axis during continental rifting is largely controlled by the rheology of the lithosphere and degree of coupling with the convecting mantle (e.g., Brune et al., 2014; Huismans and Beaumont, 2011). In addition to this, although less well understood, is the important influence that pre-existing crustal-scale structures exert on the geometry and location of intercontinental rifting and on the style of crustal deformation (e.g., Autin et al., 2013; Corti et al., 2013; Gibson et al., 2013; Schumacher, 2002; Tommasi and Vauchez, 2001).

* Corresponding author. Tel.: +44 141 330 5469.
E-mail address: m.wildman.1@research.gla.ac.uk (M. Wildman).

http://dx.doi.org/10.1016/j.tecto.2015.04.012

This phenomenon has been particularly well documented within west, central and east Africa and north-eastern Brazil where 'Pan-African' (c. 500 Ma, Frimmel, 2000) aged structures have controlled the location of Early Cretaceous intracontinental rift basins and also their subsequent inversion during the Late Cretaceous (e.g., Brown et al., 2014; Cogné et al., 2011; Daly et al., 1989; Fairhead, 1988; Raab et al., 2002; Ring, 1994; Rosendahl, 1987; Unternehr et al., 1988).

Recent structural analyses of both the on and offshore regions of the South Atlantic margin in South Africa have indeed documented evidence for multiple episodes of tectonic inversion following the initial rift phases (e.g., Andreoli et al., 1996; Brandt et al., 2003, 2005; de Beer, 2012; Hirsch et al., 2010; Kounov et al., 2009; Viola et al., 2005, 2012). Along the western margin of South Africa, however, the lack of significant or widespread post-rift sedimentary stratigraphy preserved onshore (i.e., Late Mesozoic-Tertiary) hinders detailed investigation of the timing and magnitude of post break-up tectonic development of this region of the continent. Consequently, the spatial extent and timing of these periods of tectonic activity, and the nature of any related geomorphic response, remain poorly constrained.

The origin and evolution of high passive margin topography and the longevity of the South African interior plateau (Fig. 1) have been a subject of debate for decades (Burke and Gunnell, 2008; Gilchrist and Summerfield, 1991; Gilchrist et al., 1994; Japsen et al., 2012; Moore et al., 2009; Ollier and Pain, 1997; Partridge and Maud, 1987; Paul et al., 2014; van der Beek et al., 2002). Investigations aimed at understanding the mechanisms controlling the development of this topography have focussed on assessing numerical models of the mechanical and isostatic response of the lithosphere during thinning and rupture (e.g., Brune et al., 2014; Gilchrist and Summerfield, 1991; Huismans and Beaumont, 2011; Rouby et al., 2013; ten Brink and Stern, 1992) and of syn- and post-rift mantle driven dynamic uplift (e.g., Forte et al., 2010; Gurnis et al., 2000; Lithgow-Bertelloni and Silver, 1998; Moucha and Forte, 2011; Moucha et al., 2008; Nyblade and Robinson, 1994). One of the limitations of testing these models is the paucity of useful empirical observations of the magnitude and chronology of surface uplift. One approach to resolving this limitation is constraining the timing and magnitude of major erosional events that have occurred across a particular margin using suitable empirical data, and using this information to unravel the geomorphic development of the margin.

Apatite fission track (AFT) analysis has been used extensively as a means of extracting low temperature (c. 60–110 ± 10 °C) thermal history information from rocks as they cool through the upper 3–5 km of the crust (Brown et al., 1994; Donelick et al., 2005; Gallagher et al., 1998; Lisker et al., 2009). As such, the technique has proved effective in providing constraints on the magnitude and timing of crustal denudation of the onshore regions of various rifted and continental margins where stratigraphic evidence is limited or unavailable (Gunnell et al., 2003; Japsen et al., 2006; Menzies et al., 1997; Pedersen et al., 2012). The technique has also been successfully applied to resolve the structural style of rift-margin mountains by documenting structural displacements across basement faults (e.g., Cogné et al., 2011; Foster and Gleadow, 1992; John and Foster, 1993; Redfield et al., 2005; Seward et al., 2004; Tremblay et al., 2013).

In this paper, we present new AFT and zircon fission track (ZFT) analysis data from outcrop and borehole samples. We use these data

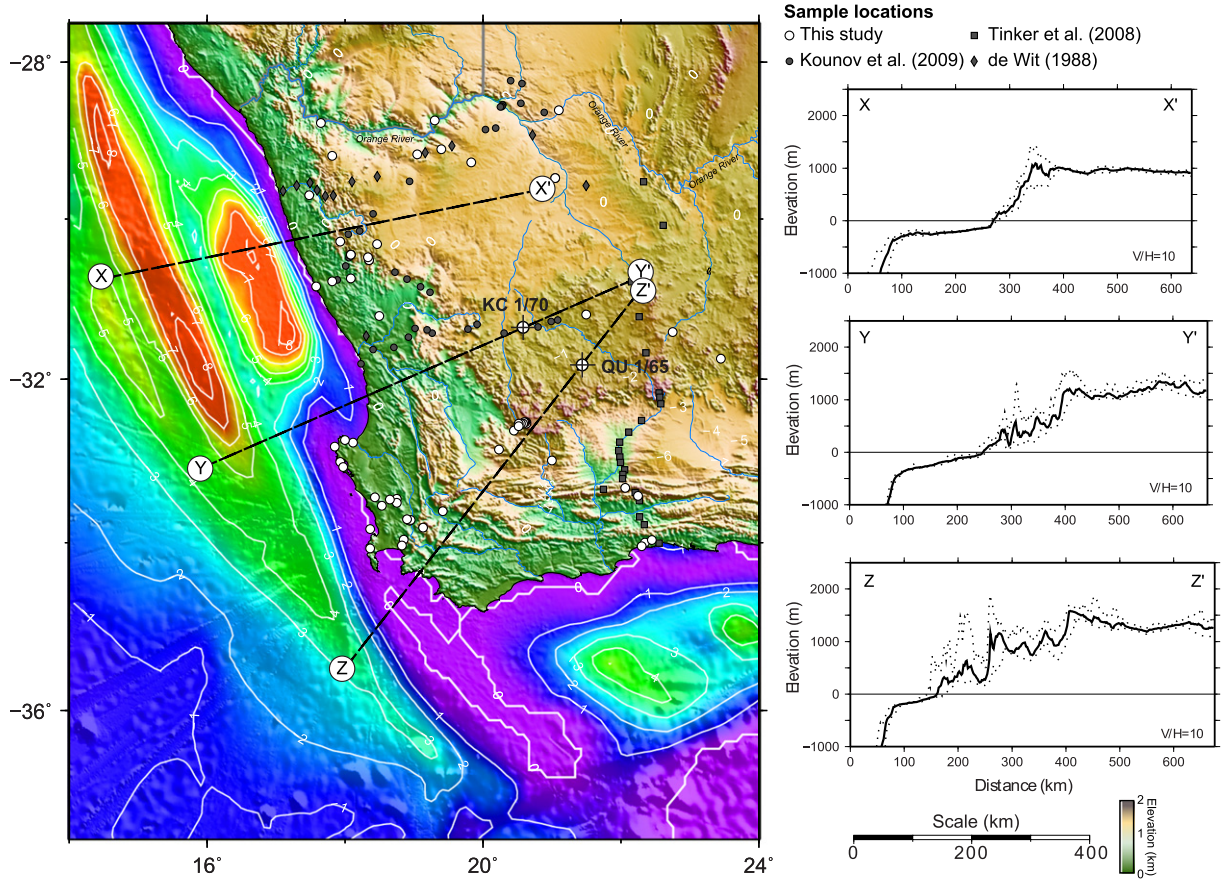

Fig. 1. Map illustrating the topography of southwestern Africa, sediment thickness in offshore basins and sample locations of regional AFT data. Regions of equal sediment thickness (data are from Rouby et al., 2009) in the offshore region are highlighted by white isopach lines and single numbers (in km). For alternative sediment thickness maps see Rouby et al. (2009) and Maystrenko et al. (2013). Three representative topographic sections across the margin are shown on the right. Elevations within 20 km of the line of section were projected. Solid line represents the mean elevation within the 40 km wide swath at 10 km windows projected onto the section while dashed lines represent the maximum and minimum values. See Supplementary material 1 (Fig. A1) for complimentary gravity and aeromagnetic maps of the region.

to quantify the low-temperature history of the crust forming the western continental margin of South Africa with a focus on the SW Cape region. The primary aim of this study is to place constraints on the timing and magnitude of long term denudation of the margin topography. The data set covers an area south of the Orange River along the continental margin and extends eastward into the interior elevated plateau to a longitude of approximately 21.5°E (Fig. 2). The data are interpreted in the context of the regional tectonic setting and augment and enhance a now extensive thermochronometry data set across this region. The implications for the timing and style of tectonics associated with the formation and development of this structurally complex continental margin are evaluated in a robust and quantitative manner using effective inversion techniques described by Gallagher (2012).

2. Regional morphology and geology

2.1. Morphology

The morphology of the SW African continental margin can be broadly described as comprising an elevated, low relief interior plateau separated from a low-lying coastal plain by a seaward facing escarpment (Fig. 1). However, along the length of the Atlantic margin, the margin morphology is highly variable. The escarpment is well defined towards the southern section of the margin where the coastal plain is flanked by a steep escarpment zone separating elevations of c. 200 m on the coastal plain to those in excess of 900 m on the plateau. Further north the escarpment starts to diminish and, instead of a prominent discrete scarp, the transition from the low lying coastal plain to an internal elevated plateau, with a mean elevation of c. 1000 m, is represented by a wider highland region, with high local relief, underlain by basement rocks that in places reach elevations greater than 1500 m (e.g., Kamiesberg).

The morphology along the southern margin, seaward of the plateau escarpment and at the SW Cape, is dominated by the remnant topography of the Permo-Triassic Cape Fold Belt (CFB) (Hälbich, 1993; Hälbich et al., 1983; Tankard et al., 2009). E–W trending ranges within the CFB reach elevations of over 2000 m in places while fault bounded basins typically form low relief, low elevation regions between the elevated ranges (e.g., Oudtshoorn and Heidelberg basins). Along the southern margin sector, the plateau escarpment is well formed and cut into the near horizontal Karoo Supergroup sedimentary rocks. The locus of the main escarpment in this area closely follows the southern outcrop limit of extensive dolerite sill intrusions suggesting a significant lithological control on the geomorphology of the escarpment in this sector at least.

2.2. Crystalline and metasedimentary basement rocks

The Namaqualand Metamorphic Province (NMP) forms the western sector of the Namaqua–Natal Metamorphic Belt which in itself represents a sector of the much more extensive Kibran (c. 1.1 Ga) orogenic province. The NMP comprise intensely deformed, high-grade gneisses with several phases of granitoid intrusion (Cornell et al., 2006; Eglington, 2006; Groenewald et al., 1991; Kröner, 1977; Tankard et al., 1982). These basement rocks have been exposed from peak metamorphic P–T conditions of 4–6 kbar (c. 12–18 km) and 700–800 °C at c. 1000–800 Ma (Dewey et al., 2006; Eglington, 2006; Robb et al., 1999; Thomas et al., 1996). They were subsequently overlain by

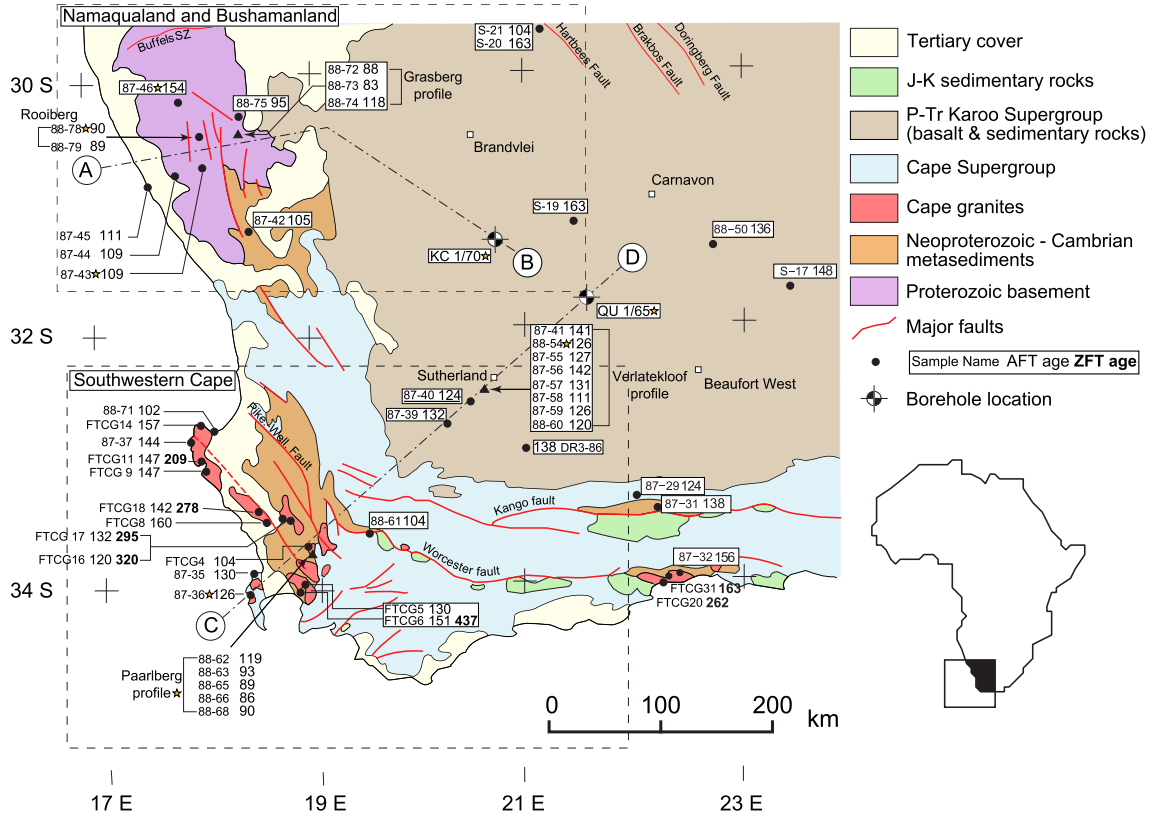

Fig. 2. Geological map of SW Africa, including major structural lineaments, with sample locations (this study only). The predominant trend of structural lineaments in the north of the study area is NW–SE characterised by the Hartbees, Brakbos and Doringberg faults. Along the South African Atlantic margin this complex fault structures have orientations deviate from this regional structural trend (e.g., prominent E–W trending Buffels River Shear Zone (Tankard et al., 2009)). At the southernmost cape the exposed Cape Granite plutons are associated with the NW–SE regional foliation, while the E–W orientation of major faults along the southern margin (e.g., Kango and Worcester faults) can be ascribed to the development of the Cape Fold Belt. An illustration of offshore faults can be seen in Fig. 3. Key samples whose thermal histories have been presented in Figs. 7, 8 and 9 have a gold star beside the sample name.

Neoproterozoic sedimentary rocks of the Gariep Supergroup and Neoproterozoic-Cambrian deposits of the Nama and Vanrhynsdorp Group. The widespread Pan-African period of orogenic activity (c. 650–480 Ma) resulted in deformation and predominantly low-grade metamorphism of these sediments and the underlying basement (Gresse et al., 2006).

Further south, the Pan-African Orogeny was accompanied by late-syntectonic localised granitoid intrusions (Groenewald et al., 1991; Stump, 1992; Tankard et al., 1982). These Early Cambrian high level plutons, termed the Cape Granite suite, are extensive in the SW Cape and are partly covered by the overlying Cape Supergroup. Thick Ordovician-Carboniferous siliciclastic sediments of the Cape Supergroup were deposited over the Cape Granites prior to Permo-Triassic crustal shortening that formed the CFB (Newton et al., 2006; Scheepers and Schoch, 2006). The compressional episode responsible for this crustal shortening has been ascribed to the subduction and accretion of the palaeo-Pacific plate beneath Gondwana (de Wit and Ransome, 1992; Tankard et al., 2009).

2.3. Sedimentary cover sequences

The Proterozoic basement is overlain by the mostly flat lying continental sediments of the Carboniferous–Late Triassic Karoo Supergroup which were deposited in a foreland basin (Karoo Basin) in front of the developing CFB (Cateneanu et al., 2005; Tankard et al., 2009). The Karoo sequence has a maximum thickness of c. 12 km, attained in the southeast of the main Karoo Basin, and thins rapidly to the north (Bumby and Guiraud, 2005; Dingle, 1982; Lindeque et al., 2007, 2011; Tankard et al., 1982). Karoo-aged sediments are also found to the northeast of the study area within fault bounded rift basins flanking the Archean Kaapvaal craton. Sedimentation within the main Karoo Basin ended in the Late Jurassic (c. 200–175 Ma) with the voluminous and extensive eruption of the Karoo tholeitic flood basalts and intrusion of associated dolerite sills and dykes (Duncan et al., 1997; Jourdan et al., 2005; Moulin et al., 2011; Svensen et al., 2012).

Although relatively minor in areal extent, an important series of Mid-Jurassic-Early Cretaceous (Oxfordian-Barremian, 160–130 Ma) sedimentary basins are preserved as narrow, E–W oriented fault bounded half graben along the southern margin of South Africa (Dingle et al., 1983; Lock et al., 1975; Viljoen, 1992). These basins preserve extensive thicknesses of coarse, poorly sorted, alluvial fan conglomerates and interbedded fluvial sandstones with occasional playa lake mudstones and silts. They rapidly thicken towards their northern margins which are bounded by major normal faults. The total thickness of sediment currently preserved thins progressively from a maximum of c. 3.1 km in Oudtshoorn basin in the east through 2.1 km for the Heidelberg basin (Viljoen, 1992), 1.2 for the Robertson basin and 0.7 km for the Worcester basin in the west (Dingle et al., 1983) (Fig. 3). The total throw on the basin bounding faults is substantial reaching c. 6 km for the Worcester fault (Dingle et al., 1983), and in the offshore extensions of some of these basins (Gamtoos and Pletmos basins) the throw (down to the south) is over 15 km (Paton, 2006; Paton et al., 2006).

No such basins are preserved onshore on the Atlantic margin to the west, but a very similar series of NNW–SSE trending fault bounded half graben basins have been inferred from interpretation of near shore seismic reflection data (Broad et al., 2012; Jungslager, 1999). These seismic reflection data and derived isopach maps possibly define an "inner graben" of the Orange basin, preserving a thickness of Jurassic-Early

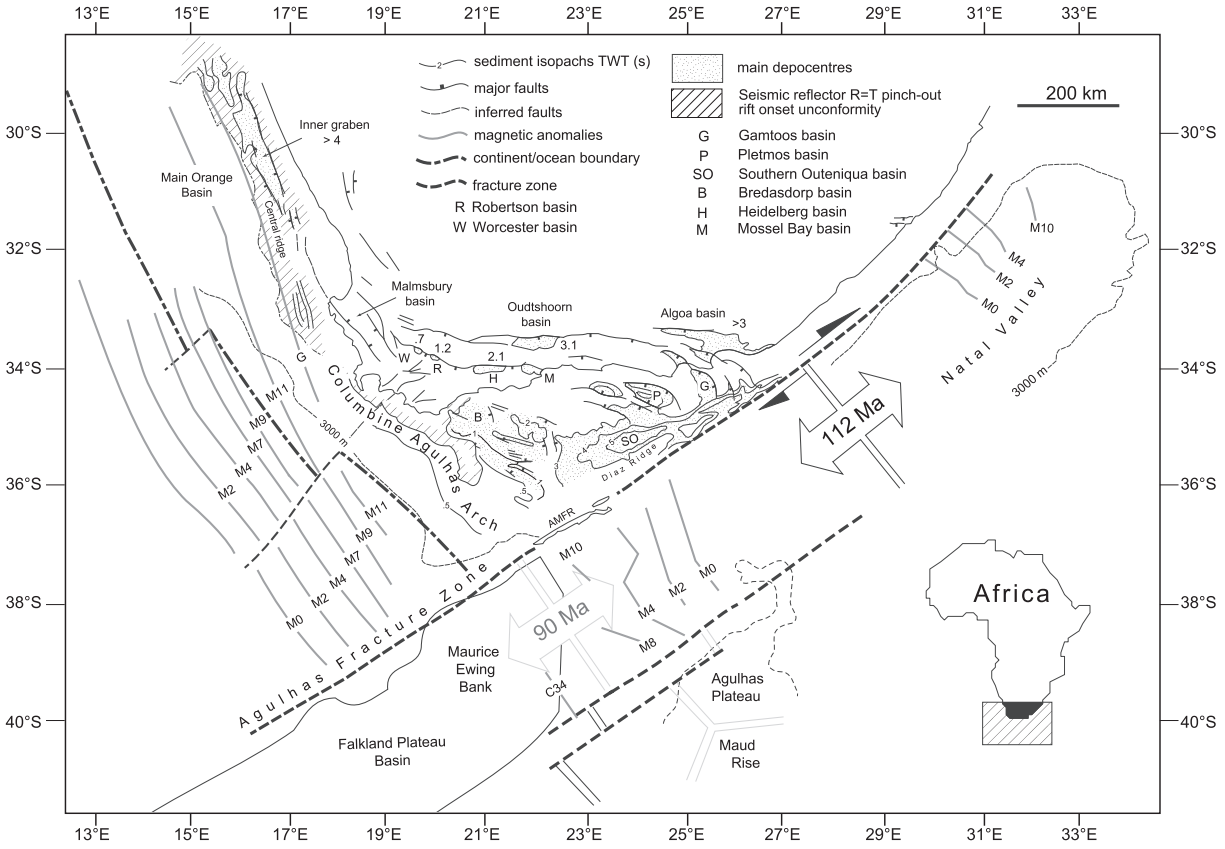

Fig. 3. Map illustrating key tectonic architecture of the SW Cape region at c. 112 Ma. The early syn-rift sedimentary basins are shown by the light stipple and the total sediment thicknesses in kilometres are indicated by the single numbers adjacent to the basin outline (and by isopachs for larger basins). White arrows indicate the position of the spreading centre at c. 112 Ma and 90 Ma.

Data sources are from Martin et al. (1982), Goodlad et al. (1982), Dingle et al. (1983), Martin and Hartnady (1986), Parsiegla et al. (2008), Nürnberg and Müller (1991), Torsvik et al. (2009).

Cretaceous sedimentary and volcanic rocks ranging from 1 km to in excess of 2.5 km (Broad et al., 2012; Dingle et al., 1983; Maystrenko et al., 2013; Rouby et al., 2009). The quality and extent of publicly available seismic data are limited though, and the exact nature, or even existence, of an inner graben is debateable. However, we believe the available seismic evidence coupled with the geophysical observations (see Supplementary Material 1) makes a strong case for an inner graben structure.

Onshore, younger Cretaceous-Tertiary sedimentary rocks mainly exist in small (c. 0.05–1.50 km^2) outcrops as outliers preserved as prominent mesas or in localised depressions in basement lithologies in the Namaqualand region (Brandt et al., 2003, 2005). Coastal Cenozoic sedimentary deposits are present over a narrow (c. 30 km wide) zone along the low coastal plain and extend along almost the entire length of the margin (e.g., de Beer, 2012; Roberts et al., 2006). Although of limited extent and exposure, the Late Cretaceous Dasdap Formation and Vaalputs sedimentary rocks described by Brandt et al. (2003, 2005) indicate the existence of significant relief and active erosion well inland of the margin at this time and the implications of this are discussed in more detail later in this paper. Fossiliferous shallow-marine sediments along the coastal plain are preserved as wave cut terraces at 90 m, 50 m, and 30 m and were deposited during cycles of marine regressions during sea-level fluctuations driven by both tectonic and eustatic processes (Roberts et al., 2006). A widespread but relatively thin (c. <300 m) Cenozoic cover is also present within the interior, northeast of the Orange River, forming the Kalahari basin (Haddon and McCarthy, 2005; Partridge et al., 2006).

2.4. Post-Karoo magmatism

The major magmatic event affecting South Africa was the extensive Mid-Jurassic Karoo igneous episode which produced voluminous continental flood basalts which covered most of southern Africa at thicknesses of at least c. 1.4 km thick (as still preserved in Lesotho) and ubiquitous intrusive dykes and sills throughout the region and especially within the main Karoo basin (Elburg and Goldberg, 2000; Jourdan et al., 2004; Marsh et al., 1997; Moulin et al., 2011). Later igneous activity on the South African sector of the Atlantic margin is limited to syn-rift igneous intrusions in the form of granitic plutons (e.g., Rietpoort granite of the Koegel Fontein intrusive complex) (Verwoerd and de Beer, 2006; Curtis et al., 2011) and mafic (mainly dolerite) dykes are present along the margin and are associated with the extensive magmatic episode that accompanied initial continental rifting during the Early Cretaceous (Jourdan et al., 2005; Reid, 1990; Reid et al., 1991; Trumbull et al., 2007). Subsequent magmatism is represented by numerous and widespread, but volumetrically minor, kimberlite and alkaline intrusive rocks. Kimberlite intrusions have been subdivided into two distinct age groups based on both age and mineralogical characteristics: Type II kimberlites that have continental lithosphere geochemical affinities and emplacement ages between 145 and 111 Ma and Type I kimberlites that have depleted mantle affinities and ages between 95 and 80 Ma (e.g., Basson and Viola, 2004; Smith et al., 1985). Non-kimberlite intrusions are predominantly Late Cretaceous–Tertiary olivine melilitites that form shallow intrusive pipes, sills and dykes emplaced during separate events to that of kimberlite volcanism (Moore and Verwoerd, 1985; Verwoerd and De Beer, 2006). For a comprehensive collation of the timing and location of alkaline igneous intrusive bodies, the user is referred to Moore et al. (2008) and Jelsma et al. (2009).

3. Tectonic setting

3.1. Regional tectonic architecture and structures

The predominant trend of structural lineaments along the South African Atlantic margin is NW–SE to NNW–SSE, but is characterised in some areas by sets of complex faults with orientations deviating from the regional structural trend (Fig. 2). South of the Orange River (c. 100 km), the NMP basement rocks of the Namaqualand region are dissected by numerous structural lineaments, including the prominent E–W trending Buffels River Shear Zone (Tankard et al., 2009). These structural lineaments predominantly trend NNW–SSE, with a significant number of major high angle N–S trending faults, and show top-to-the-west normal displacement (Viola et al., 2012). It has been suggested that Late Mesozoic-Cenozoic reactivation has occurred on some of these structures while neotectonic activity has also been documented along the Namibian margin (White et al., 2009) southwest African margin (Andreoli et al., 1996; Brandt et al., 2005; de Beer, 2012) and in the adjacent offshore Atlantic basins (Viola et al., 2005).

Towards the southwestern tip of Africa, the SW Cape region has experienced several major tectonic episodes, including three tectonic inversions during the Phanerozoic (de Wit and Ransome, 1992; Paton, 2006; Paton and Underhill, 2004; Thomson, 1999). Prior to continental breakup, the SW Cape lay near the southern margin of the Gondwana supercontinent adjacent to the future point of rifting and separation. Fracture of the southern edge of Gondwana took place parallel to the NW–SE structural grain of the Late-Proterozoic Pan-African metasedimentary basement rocks. Several major fault zones (Figs. 2, 3) show a close parallelism with the NW–SE coastline and hence the axis of rifting. At least two of these fault zones represent discontinuities in the basement rocks and have been interpreted as terrain boundaries (Hartnady et al., 1974; Tankard et al., 1982, 2009). Some of the major structures within the CFB were reactivated as major normal faults during rifting in the Mesozoic and an E–W array of local Newark-type basins formed within evolving half graben in the Mid-Jurassic-Early Cretaceous (Oxordian-Barremian) (Fig. 3) (Dingle et al., 1983; Lock et al., 1975; Paton, 2006; Paton and Underhill, 2004; Paton et al., 2006; Viljoen, 1992).

Structural trends along the South Atlantic margin are believed to exert a strong control over the occurrence of intrusive igneous rocks, particularly in the SW Cape where the widely exposed Cape Granite plutons tend to be elongated parallel to the NW–SE trend of the regional foliation (Fig. 2). Also, dolerite dyke swarms associated with rifting of the South Atlantic trend NW–SE (Day, 1987; Reid, 1990; Reid et al., 1991; Trumbull et al., 2007) and provide evidence of regional extensional fracturing along pre-existing crustal structures. Major tectonic episodes and the occurrence of structural discontinuities may also have had a significant control on the occurrence of the numerous Cretaceous and younger kimberlite intrusions found across South Africa (e.g., Jelsma et al., 2009; Reid, 1990). Recent work has shown that these prominent NW–SE trending fault zones extend far into the offshore basins around the south-western coast of Africa (de Vera et al., 2010; Viola et al., 2005).

3.2. Chronology of rifting: break-up, magmatism and rift flank uplift

Transtensional intracontinental rifting heralded the Mid-Late Jurassic separation of East Gondwana (Antarctica–India–Madagascar) from West Gondwana (Africa–South America) at c. 165–150 Ma (Cateneanu et al., 2005; Delvaux, 2001; Rosendahl, 1987). The earlier onset of intracontinental rifting has been linked to the Karoo igneous episode (Courtillot et al., 1999; Cox, 1992; Richards et al., 1989; White and McKenzie, 1989) at c. 185–177 Ma (Duncan et al., 1997; Jourdan et al., 2007; Moulin et al., 2011; Svensen et al., 2012).

The identification of magnetic anomalies aged c. 135–130 Ma, provides a likely minimum age for the onset of significant dextral movement along the Falkland–Agulhas Fracture Zone (FAFZ) (Jokat et al., 2003; König and Jokat, 2006, 2010; Kovacs et al., 2002; Tikku et al., 2002). Evidence for an earlier rifting phase is preserved within the deep, half-graben basins along the southern margin of South Africa (Algoa, Gamtoos, Pletmos) that preserve thick, terrestrial syn-rift sequences (>10 km) of coarse clastic sediments and basaltic lavas dating back to the Oxfordian (c. 163–157 Ma) (Paton, 2006; Paton et al.,

Table 1
Summary of fission track analysis results.

Sample no.	Lithology	Stratigraphic age	Longitude	Latitude	Depth or elev. (m)	Xtals	ρ_s	N_s	ρ_i	N_i	$P\chi^2$%	ρ_d	N_d	Mineral	FT age (Ma) ± 1σ	Mean length (μm) ± 1σ	Std. dev. (μm)	N
Namaqualand and Bushmanland					*Elev (m)*													
8732-50	hbl-bt-gneiss (Kleinsee)	Mid-Proterozoic	17.483	−29.700	50	15	0.682	(756)	1.333	(1478)	80.7	1.295	(5435)	Ap	115 ± 6	14.08 ± 0.16	0.99	(36)
8732-51[a]	bt-migmatite-gneiss	Mid-Proterozoic	17.817	−29.200	970	20	1.336	(1824)	4.736	(6466)	0.3	2.344	(9958)	Ap	117 ± 6	13.70 ± 0.18	1.45	(63)
8732-52[a]	hbl-bt-granite-gneiss	Mid-Proteozoic	17.650	−28.783	190	20	0.548	(734)	2.28	(3052)	0	2.344	(9958)	Ap	108 ± 7	12.93 ± 0.50	1.86	(14)
8732-86	hbl-bt-gneiss (Onseepkans crossing, Orange R.)	Mid-Proterozoic	19.300	−28.750	420	22	1.061	(1573)	4.145	(6148)	0	2.344	(9958)	Ap	114 ± 7	13.47 ± 0.15	1.42	(85)
8732-87	bt-gneiss (34.8 km W of Poffader)	Mid-Proterozoic	19.050	−29.183	870	15	0.633	(551)	1.358	(1183)	23.6	1.295	(5435)	Ap	105 ± 6	14.07 ± 0.19	1.24	(44)
8732-88	Augen-bt-gneiss (Poffader township)	Mid-Proterozoic	19.400	−29.117	900	15	1.904	(1326)	4.101	(2856)	22.6	1.295	(5435)	Ap	104 ± 4	13.73 ± 0.13	1.34	(100)
8732-93	bt-gneiss (22.2 km SW of Upington on R64)	Mid-Proterozoic	21.100	−28.617	700	20	0.815	(852)	2.018	(2111)	28.4	1.295	(5435)	Ap	91 ± 4	13.97 ± 0.11	1.09	(94)
NF-008	bt-gneiss	Mid-Proterozoic	19.833	−29.283	~950	26	0.308	(680)	0.731	(1611)	25	1.262	(7331)	Ap	92 ± 9	13.17 ± 0.30	2.21	(54)
S-20	fg-sst (Ecca Fm)	Lower-Permian	21.050	−29.483	900	20	1.819	(1989)	3.873	(4235)	0	1.13	(5309)	Ap	99 ± 5	13.82 ± 0.26	1.96	(57)
S-21	bt-granite (Draghoender granite)	Early Proterozoic	22.200	−29.450	1010	20	0.298	(214)	0.572	(411)	75.1	1.154	(5309)	Ap	104 ± 9	13.97 ± 0.37	1.67	(20)
8732-42[a]	Porphyritic-granite-gneiss	Mid-Proterozoic	18.500	−31.217	370	20	1.147	(1741)	2.458	(3732)	0	1.296	(12,343)	Ap	105 ± 4	13.36 ± 0.25	2.51	(100)
8732-43[a]	Porphyritic-granite-gneiss	Mid-Proterozoic	18.083	−30.750	300	20	0.531	(899)	1.788	(3027)	65.2	2.344	(9958)	Ap	121 ± 5	13.44 ± 0.22	1.36	(37)
8732-44[a]	Porphyritic-granite-gneiss	Mid-Proterozoic	17.817	−30.783	100	20	1.658	(2144)	6.18	(7990)	17.9	2.344	(9958)	Ap	109 ± 3	13.34 ± 0.13	1.36	(115)
8732-45[a]	bt-gneiss (Groen Rivier Mond)	Mid-Proterozoic	17.583	−30.850	0	19	1.339	(652)	2.72	(1324)	92.3	1.296	(12,343)	Ap	111 ± 6	12.75 ± 0.25	2.47	(100)
8732-46[a]	Felsic-gneiss	Mid-Proterozoic	17.933	−30.283	750	21	1.205	(2094)	3.128	(5434)	0	2.344	(9958)	Ap	154 ± 7	13.30 ± 0.15	1.6	(116)
8832-72	bt-gneiss (Grasberg summit trig. station, 1335 m)	Mid-Proterozoic	18.350	−30.517	1335	20	0.405	(221)	0.779	(425)	68.2	0.97	(4441)	Ap	88 ± 8	13.68 ± 0.48	1.58	(11)
8832-73	bt-augen-gneiss (On track from Grasberg summit)	Mid-Proterozoic	18.350	−30.517	1180	20	1.274	(1082)	2.599	(2207)	9.1	0.972	(4441)	Ap	83 ± 4	13.62 ± 0.20	2.07	(102)
8832-74	bt-augen-gneiss (from stream bed below Grasberg)	Mid-Proterozoic	18.333	−30.483	1000	20	0.977	(802)	1.398	(1148)	25.5	0.974	(4441)	Ap	118 ± 6	13.66 ± 0.30	2.08	(47)
8832-75	Felsic-bt-gneiss (4 km W of Platbakkies)	Mid-Proterozoic	18.467	−30.317	1030	20	1.405	(1731)	2.66	(3278)	5.2	0.976	(4441)	Ap	95 ± 4	13.46 ± 0.33	2.03	(39)
8832-78	Amphibolite (mafic dyke?) (Rooiberg)	Mid-Proterozoic	18.083	−30.450	1620	20	1.727	(1228)	3.304	(2349)	20.2	0.979	(4441)	Ap	89 ± 4	13.14 ± 0.20	2.01	(104)
8832-79	Amphibolite (mafic dyke?) (Rooiberg)	Mid-Proterozoic	18.083	−30.450	1500	20	0.766	(1078)	1.455	(2048)	64.8	0.981	(4441)	Ap	90 ± 4	13.99 ± 0.36	1.57	(19)
Southwestern Cape					*Elev (m)*													
8732-29	Quartzite (Table Mountain Gp.)	Siluro-Ordovician	22.067	−33.333	1600	22	1.159	(768)	4.581	(3036)	0	2.344	(9958)	Ap	124 ± 12	13.78 ± 0.21	0.74	13
8732-31	Granite (boulders from meta-diamictite)	Late-Proterozoic	22.25	−33.433	550	20	0.67	(391)	1.973	(1152)	14.8	2.344	(9958)	Ap	138 ± 8	13.2 ± 0.22	1.74	63
8732-32	cg-porphyritic-bt-granite (George pluton)	Cambrian	22.35	−34	100	20	1.445	(2459)	3.748	(6379)	16.6	2.344	(9958)	Ap	156 ± 5	13.86 ± 0.12	1.21	102
8732-34[a]	mg-bt-granite (Cape granite suite)	Cambrian	19.133	−33.817	450	25	2.685	(3102)	3.844	(4442)	77.6	1.296	(12,343)	Ap	157 ± 5	12.93 ± 0.22	2.43	(125)
8732-35[a]	mg-bt-granite (Paarlberg granite)	Cambrian	18.367	−33.833	300	22	1.666	(1121)	2.874	(1934)	57	1.296	(12,343)	Ap	130 ± 5	12.82 ± 0.20	2.01	(100)
8732-36[a]	Porphyritic-granite (Chapmans Peak drive)	Cambrian	18.367	−34.067	150	20	4.287	(4529)	7.918	(8365)	0.2	1.296	(12,343)	Ap	126 ± 4	14.20 ± 0.22	0.96	(100)
8732-37[a]	cg-prphtc-granite (Cape Columbine)	Cambrian	17.850	−32.833	0	25	0.613	(746)	0.956	(1163)	87.7	1.296	(12,343)	Ap	144 ± 7	13.38 ± 0.23	2.02	(75)
8832-50	vfg-sst (L. Beaufort Gp., 43 km W Loxton)	Permian	29.983	−28.983	1300	22	1.154	(486)	1.615	(680)	41	1.094	(4423)	Ap	136 ± 9	13.21 ± 0.31	2.46	62
8832-61	bt-granite (Worcester fault zone)	Cambrian	19.417	−33.617	290	20	0.414	(332)	0.866	(694)	75.6	0.126	(4423)	Ap	104 ± 7	13.04 ± 0.43	1.68	(15)

(continued on next page)

Table 1 (*continued*)

Sample no.	Lithology	Stratigraphic age	Longitude	Latitude	Depth or elev. (m)	Xtals	ρ_s	N_s	ρ_i	N_i	$P\chi^2$%	ρ_d	N_d	Mineral	FT age (Ma) ± 1σ	Mean length (μm) ± 1σ	Std. dev. (μm)	N
8832-71	vcg-bt-granite (West Point, St Helena Baai)	Cambrian	18.117	−32.783	0	20	0.446	(456)	0.737	(753)	61.9	0.968	(4441)	Ap	102 ± 6	13.60 ± 0.29	2.38	(65)
DR3/86	mg-felspathic-sst (L. Beaufort Gp.)	Permian	21.000	−33.000	900	20	1.785	(924)	3.106	(1608)	59.9	1.39	(7635)	Ap	138 ± 6	14.12 ± 0.34	2	(35)
S-17	fg-felspathic-sst (U. Beaufort Gp.)	Lower-Triassic	23.45	−31.75	1190	20	1.197	(583)	1.546	(753)	82.2	1.108	(5309)	Ap	148 ± 9	13.5 ± 0.34	2.63	57
S-19	mg-felspathic-sst (L. Beaufort Gp.)	Permian	21.500	−31.200	1270	20	0.793	(729)	0.959	(882)	20.9	1.142	(5309)	Ap	163 ± 9	13.37 ± 0.30	3.03	(100)
FTCG 04	Cape granites	Cambrian	18.900	−33.717	670	20	0.647		1.489	(1145)	30	1.391	(9637)	Ap	119 ± 9	12.53 ± 0.38	1.63	(24)
FTCG 05	Cape granites	Cambrian	18.853	−33.963	130	20	2.377	(2043)	4.379	(3763)	30	1.391	(9637)	Ap	130	±4	13.67	±0.41
FTCG 06	Cape granites	Cambrian	18.825	−34.033	100	15	1.466	(945)	2.331	(1502)	15	1.391	(9637)	Ap	151 ± 6	13.33 ± 0.40	1.57	(85)
						8	2.22	(1508)	0.108	(73)	40	3.343	(2317)	Zr	**437 ± 53**			
FTCG 08	Cape granites	Cambrian	18.533	−33.550	90	20	1.303	(818)	1.951	(1225)	10	1.391	(9637)	Ap	160 ± 7	13.57 ± 0.41	1.32	(69)
FTCG 09	Cape granites	Cambrian	17.975	−33.083	20	10	4.014	(1391)	6.606	(2289)	<1	1.391	(9637)	Ap	147 ± 10	12.90 ± 0.39	1.52	(100)
FTCG 10	Cape granites	Cambrian				2	3.03	(546)	0.266	(48)	65	3.343	(2317)	Zr	**244 ± 37**			
FTCG 11	Cape granites	Cambrian	17.933	−33.021	10	20	2.757	(1605)	4.492	(2615)	60	1.391	(9637)	Ap	147 ± 5	13.32 ± 0.40	1.28	(100)
						2	2.494	(484)	0.258	(50)	15	3.343	(2317)	Zr	**209 ± 31**			
FTCG 14	Cape granites	Cambrian	18.000	−32.750	10	7	0.978	(267)	1.483	(405)	80	1.391	(9637)	Ap	157 ± 12	13.61 ± 0.41	1.29	(100)
FTCG 16	Cape granites	Cambrian	18.750	−33.517	210	20	1.08	(952)	2.165	(1908)	15	1.391	(9637)	Ap	120 ± 5	12.86 ± 0.39	1.61	(100)
						12	1.837	(2292)	0.123	(153)	60	3.343	(2317)	Zr	**320 ± 27**			
FTCG 17	Cape granites	Cambrian	18.650	−33.475	300	20	2.221	(2616)	4.017	(4732)	15	1.391	(9637)	Ap	132 ± 4	13.00 ± 0.39	1.82	(100)
						3	3.13	(911)	0.227	(66)	10	3.343	(2317)	Zr	**295 ± 38**			
FTCG 18	Cape granites	Cambrian	18.433	−33.450	150	20	4.62	(3554)	7.826	(6020)	<1	1.391	(9637)	Ap	142 ± 4	13.12 ± 0.39	1.51	(100)
						2	3.626	(402)	0.28	(11)	60	3.343	(2317)	Zr	**278 ± 52**			
FTCG 20	cg-porphyritic-bt-granite (George pluton)	Cambrian	22.300	−34.042	0	5	1.84	(714)	0.142	(55)	<1	3.343	(2317)	Zr	**262 ± 53**			
FTCG 31	cg-porphyritic-bt-granite (George pluton)	Cambrian	22.450	−33.967	200	10	1.419	(2458)	0.189	(327)	90	3.343	(2317)	Zr	**163 ± 10**			
Borehole and profile samples																		
QU 1/65					*Depth (m)*													
Quagga's Fontein																		
8732-95	mg-felspathic-sst (L. Beaufort Gp.)	Permian	21.439	−31.826	11	20	0.702	(751)	0.962	(1030)	23.8	1.026	(3427)	Ap	130 ± 7	13.78 ± 0.18	1.8	(100)
QU 335	Grey-fg-felspathic-sst (L. Beaufort Gp.)	Permian	21.439	−31.826	103	20	0.56	(483)	0.927	(799)	25.4	1.07	(3427)	Ap	112 ± 7	13.48 ± 0.19	1.92	(100)
QU 741	Grey-fg-felspathic-sst (L. Beaufort Gp.)	Permian	21.439	−31.826	228	11	0.532	(186)	0.869	(304)	16.9	1.077	(3427)	Ap	114 ± 11	–	–	–
8732-96[a]	Grey-fg-felspathic-sst (L. Beaufort Gp.)	Permian	21.439	−31.826	397	20	1.14	(520)	1.191	(872)	91.3	1.262	(7331)	Ap	130 ± 8	13.18 ± 0.30	2.12	(50)
8732-98[a]	Grey-fg-felspathic-sst (Ecca Gp.)	Lower-Permian	21.439	−31.826	925	22	1.517	(685)	2.943	(1329)	29	1.296	(12,343)	Ap	116 ± 6	13.03 ± 0.29	2.09	(52)
8732-97	Grey-fg-felspathic-sst (Ecca Gp.)	Lower-Permian	21.439	−31.826	1358	17	0.686	(255)	1.493	(555)	27.2	1.033	(3427)	Ap	83 ± 7	13.00 ± 0.40	1.81	(21)
8732-100	Diamictite (Dwyka Fm.)	Carboniferous	21.439	−31.826	1942	20	0.371	(601)	1.385	(2246)	0	1.048	(3427)	Ap	45 ± 4	11.23 ± 0.56	3.63	(42)
8732-101	Diamictite (Dwyka Fm.)	Carboniferous	21.439	−31.826	2148	20	0.156	(231)	0.92	(1326)	0	1.055	(3427)	Ap	30 ± 8	9.64 ± 0.37	2.81	(56)
8732-102	Diamictite (Dwyka Fm.)	Carboniferous	21.439	−31.826	2318	20	0.086	(113)	0.359	(474)	65.3	1.062	(3427)	Ap	44 ± 5	10.72 ± 0.54	2.82	(27)
8732-103	vcg-porphyritic-bt-granite	Cambrian	21.439	−31.826	2435	15	0.317	(264)	4.382	(3650)	0	1.295	(5435)	Ap	16 ± 2	9.93 ± 0.35	2.56	(53)
8732-105[a]	vcg-porphyritic-bt-granite	Cambrian	21.439	−31.826	2545	20	0.225	(333)	4.456	(6602)	0.5	1.299	(7331)	Ap	11 ± 1	9.83 ± 0.42	2.71	(41)

KC 1/70 Leeuweriet (Klip Cypher)					*Depth (m)*													
KC-1	Cuttings: grey-fg-mdst (Ecca Fm.)	Lower-Permian	20.583	−31.358	222	18	0.145	(162)	0.187	(209)	97.9	1.084	(3427)	Ap	146 ± 16	13.77 ± 0.38	2.27	(35)
KC-3	Cuttings: grey-fg-mdst (Ecca Fm.)	Lower-Permian	20.583	−31.358	838	18	0.282	(262)	0.375	(348)	95.5	1.091	(3427)	Ap	142 ± 12	13.90 ± 0.39	1.52	(15)
KC-6	Cuttings: bt-gneiss	Mid-Proterozoic	20.583	−31.358	1608	19	0.271	(246)	0.637	(579)	70.1	1.099	(3427)	Ap	81 ± 6	12.58 ± 0.24	1.72	(53)
KC-8	Cuttings: bt-gneiss	Mid-Proterozoic	20.583	−31.358	2178	20	0.481	(846)	1.56	(2742)	18.1	1.106	(3427)	Ap	60 ± 3	11.94 ± 0.14	1.38	(101)
KC-21	Cuttings: bt-gneiss	Mid-Proterozoic	20.583	−31.358	6190	4	0	(0)	2.409	(1125)	–	1.113	(3427)	Ap	0 –	–	–	–
Borehole and profile samples																		
Paarlberg					*Elev (m)*													
8832-62	Porphyritic-bt-granite (Paarlberg pluton)	Cambrian	18.917	−33.725	729	20	0.555	(421)	1.071	(812)	9.2	1.275	(4423)	Ap	119 ± 9	13.46 ± 0.39	1.66	(18)
8832-63	Porphyritic-bt-granite (Paarlberg pluton)	Cambrian	18.925	−33.725	630	20	0.792	(426)	1.917	(1031)	72.4	1.295	(4423)	Ap	93 ± 6	14.63 ± 0.21	0.55	(7)
8832-65	Porphyritic-bt-granite (Paarlberg pluton)	Cambrian	18.942	−33.733	450	20	0.529	(369)	1.354	(945)	65.9	1.316	(4423)	Ap	89 ± 6	14.13 ± 0.17	1.03	(35)
8832-66	Porphyritic-bt-granite (Paarlberg pluton)	Cambrian	18.953	−33.725	320	15	0.514	(206)	1.392	(558)	82.5	1.336	(4423)	Ap	86 ± 7	13.32 ± 0.35	0.49	(2)
8832-68	Porphyritic-bt-granite (Paarlberg pluton)	Cambrian	18.750	−33.467	125	20	0.38	(324)	0.992	(845)	87.1	1.356	(4423)	Ap	90 ± 6	13.62 ± 0.38	1.26	(11)
Verlatekloof					*Elev (m)*													
8832-54	fg to mg-felspathic-sst (L. Beaufort Gp.)	Permian	20.633	−32.550	1658	20	1.034	(848)	1.58	(1296)	25.3	1.114	(4423)	Ap	126 ± 6	13.73 ± 0.30	1.55	(55)
8732-41[a]	fg to mg-felspathic-sst (L. Beaufort Gp.)	Permian	20.633	−32.533	1550	30	0.875	(1495)	1.482	(2534)	3.3	1.296	(12,343)	Ap	141 ± 6	13.56 ± 0.14	1.83	(170)
8832-55	fg to mg-felspathic-sst (L. Beaufort Gp.)	Permian	20.617	−32.533	1430	20	1.281	(786)	1.981	(1215)	93	1.134	(4423)	Ap	127 ± 6	13.02 ± 0.30	2.1	(48)
8832-56	fg to mg-felspathic-sst (L. Beaufort Gp.)	Permian	20.600	−32.533	1290	20	1.112	(719)	1.566	(1013)	53.4	1.155	(4423)	Ap	142 ± 8	13.55 ± 0.17	1.65	(100)
8832-57	fg to mg-felspathic-sst (L. Beaufort Gp.)	Permian	20.583	−32.550	1190	20	1.811	(966)	3.022	(1612)	0.5	1.172	(4423)	Ap	131 ± 8	13.18 ± 0.29	1.58	(32)
8832-58	fg to mg-felspathic-sst (L. Beaufort Gp.)	Permian	20.550	−32.550	1090	20	1.361	(567)	2.537	(1057)	37.7	1.195	(4423)	Ap	111 ± 7	12.81 ± 0.27	2.13	(64)
8832-59	fg to mg-felspathic-sst (L. Beaufort Gp.)	Permian	20.517	−32.550	980	20	0.729	(515)	1.216	(859)	77.5	1.215	(4423)	Ap	126 ± 8	13.30 ± 0.30	1.78	(35)
8732-39[a]	fg to mg-felspathic-sst (L. Beaufort Gp.)	Permian	20.233	−32.867	880	32	0.988	(681)	3.045	(2098)	93.4	2.344	(9958)	Ap	132 ± 6	13.38 ± 0.16	1.47	(88)
8832-60	fg to mg-felspathic-sst (L. Beaufort Gp.)	Permian	20.517	−32.583	850	20	0.677	(525)	1.205	(934)	84.1	1.235	(4423)	Ap	120 ± 7	13.10 ± 0.27	2.17	(65)
8732-40[a]	fg to mg-felspathic-sst (L. Beaufort Gp.)	Permian	20.450	−32.633	730	28	0.854	(940)	2.804	(3086)	88	2.344	(9958)	Ap	124 ± 5	13.48 ± 0.14	1.85	(170)

Apatite ages calculated using a zeta of 350.2 ± 5 for NBS glass SRM 612. Measured values of ri were multiplied by a geometry factor of 2 to calculate the age. The mean crystal age is reported where $P(\chi^2) < 5\%$.
ρ_s—measured spontaneous track density: N_s—number of spontaneous tracks counted.
ρ_i—measured induced track density: N_i—number of induced tracks counted.
$P(\chi^2)$—probability of obtaining observed χ^2 value for n degrees of freedom (n = number of crystals − 1).
ρ_d—track density measured in external detector adjacent to the glass dosimeter during irradiation. N_d—number of tracks counted in determining rd.
[a] Data from Brown et al. (1990).

2006). These basins were formed by tectonic reactivation of steep faults related to the earlier CFB orogenic phase (280–240 Ma) and indicate that significant displacement was taking place between the Falkland Plateau and southern Africa at this time (Paton, 2006; Paton et al., 2006; Tankard et al., 2009).

The dextral motion and resulting transtensional stresses along the FAFZ were responsible for the formation of the early syn-rift basins preserved offshore along the southern margin (Paton et al., 2006; Tankard et al., 2009) and onshore as deeply eroded remnants within the CFB. The main elements of the tectonic architecture of the southern margin and the SW Cape are illustrated in Fig. 3 for a reconstruction to the base Late Cretaceous (c. 112 Ma). In the context of this work the timing of when the continental Falkland Plateau clears the SW Cape (at c. 105 Ma) is important, because it effectively marks the final separation of continental South America and Africa and merging of the South Atlantic and Southern Ocean basins. The related timing of ridge migration past the SW Cape may coincide with the voluminous basaltic volcanism that formed the Agulhas Plateau (c. 120–90 Ma) just to the south (Marks and Tikku, 2001; Parsiegla et al., 2008; Uenzelmann-Neben and Gohl, 2004).

The detailed chronology of rifting in the South Atlantic and the subsequent geometry and plate kinematics within the South Atlantic basin has been well studied (e.g., Cande et al., 1988; Eagles, 2007; Nürnberg and Müller, 1991), and has been the focus of recent attention (Aslanian and Moulin, 2013; Koopmann et al., 2013; Torsvik et al., 2009). We direct readers to these studies and references therein for detailed discussion of this topic. For this work it is sufficient to note that, despite some minor differences, there is consensus that initial rifting began around c. 165 Ma and final break-up, heralded by formation of true oceanic crust between South America and Africa, occurred diachronously starting at c. 130 ± 5 Ma in the south and propagated northwards where the earliest sea floor identified offshore in northern Namibia is c. 128 Ma (Koopmann et al., 2013; Nürnberg and Müller, 1991) (Fig. 3). Breakup in the South Atlantic was also accompanied by voluminous eruption of continental flood basalts and rhyolites (Hawkesworth et al., 2000; Peate, 1997; Trumbull et al., 2007) and accompanying dyke swarms, granitoid and alkaline igneous intrusions (Almeida et al., 2013; Day, 1987; Milner et al., 1993; Reid, 1990; Reid and Rex, 1994; Reid et al., 1991; Schmitt et al., 2000; Watkins et al., 1994) making up the Paraná–Etendeka continental flood basalt province which is exposed in SE Brazil and N Namibia.

After breakup, sea floor spreading within the Natal Valley and the South Atlantic progressed steadily and symmetrically at rates of 6 cm/yr for 40 Ma or so until a major excursion in the plate kinematics of the South Atlantic and Western Indian Oceans took place between anomalies C34 and C24 (c. 84–56 Ma). This excursion involved a major change in spreading direction between Africa and South America and a similar change between Antarctica and Africa and a rapid decrease in spreading rate in the South Atlantic from 6 cm/Ma at c. 84 Ma to 2.5 cm/yr at c. 56 Ma (Gaina et al., 2013; Torsvik et al., 2009). After chron C24 (c. 56 Ma) time plate motions returned to their pre-C34 geometry, and spreading rates on the South Atlantic ridge returned to c. 6 cm/yr by c. 45 Ma (Cande and Stegman, 2011; Cande et al., 1988).

4. Fission track analysis results

A total of 59 outcrop samples were collected across the study area. Sample details, AFT and ZFT analytical results are summarised in Table 1. To aid presentation and interpretation, the data have been subdivided into two broad regional groups (Fig. 2). From Namaqualand and Bushmanland, 21 outcrop samples were collected from the Proterozoic basement and one from an outcrop of lower Permian Karoo sandstone. These samples were mainly collected across the high relief Namaqualand escarpment and Orange River valley. The Southwestern Cape dataset comprises 38 outcrop samples, of which, five forms the Paarlberg vertical topographic profile. Five samples were collected from cuttings from the KC 1/70 borehole and 11 core samples from the QU 1/65 borehole. A vertical profile over 2500 m was obtained from the QU 1/65 borehole located at Quaggas Fontein, 200 km inland of the escarpment, whereas the KC 1/70 borehole extends to a depth of 6000 m but has been more sparsely sampled over this range. The remaining outcrop samples were mostly collected from the granitic plutons of the Cape Granite suite apart from S-19 (Lower Triassic Beaufort Group sandstone) and DR3/86 (Permian Beaufort Group sandstone). For details on analytical methodology and radial plots of AFT single grain ages, see Supplementary material 2.

4.1. Apatite fission track results

4.1.1. Namaqualand and Bushmanland

Apart from sample S-20 which was collected from a Lower Permian Karoo Supergroup sandstone, all samples from this region where collected from the NMP basement rocks. The elevation of these range from sea level (0 m) to 1620 m. AFT ages ranging from 83 ± 4 Ma (8832-73) to 154 ± 7 Ma (8732-46) and show no clear correlation with elevation (Fig. 4). Although there is also no correlation between age and elevation it is interesting to note that some of the youngest AFT ages were obtained from the highest elevations. Mean track lengths (MTLs) vary between 12.75 ± 0.25 μm (8732-45) to 14.08 ± 0.16 μm (8732-50) with track length distributions (TLDs) being predominantly unimodal. Several samples do, however, have single grains with ages of c. 60–70 Ma and have distinct tails of highly annealed tracks (see samples S-20, 8732-42, 8832-75, 8832-73). There is no clear relationship between the apparent AFT age and MTL (Fig. 5) suggesting that these samples have experienced a complicated thermal history.

The predominantly Early Cretaceous AFT ages and the relatively narrow, unimodal TLDs with MTLs between c. 13 and 14 μm, suggest that many of the samples initially cooled from elevated palaeotemperatures in excess of 110 ± 10 °C during the Early Cretaceous. However, the common occurrence of single grain ages as young as 54 Ma (8832-72) and the presence of a significant number of highly annealed tracks within some of the TLDs, particularly within older samples, indicates that cooling to surface temperatures was initially protracted and was probably not completed until the Late Cretaceous. In contrast, most of the remaining samples probably first cooled to below 110 ± 10 °C during the Early Cretaceous (c. 150–130 Ma). The unimodal TLDs and generally long MTLs (i.e., >13 μm) observed for samples with ages ranging from circa 150 Ma to 80 Ma suggest that these ages represent a discrete cooling episodes at different times.

Apart from the occurrence of small, isolated alkaline intrusives (Marsh, 1973; Moore, 1976; Moore and Verwoerd, 1985) described above there is no evidence for widespread magmatic activity during the Late Cretaceous within the Namaqualand and Bushmanland area. Assuming that palaeogeothermal gradients were similar to present day values of c. 20–25 °C/km (Ballard and Pollack, 1987; Jones, 1987) then at least 3 or 4 km of denudation are implied over much of this region with variations in timing and amount likely to have been caused by structurally controlled displacement and differential uplift across major faults. Even if palaeogeothermal gradients were abnormally high during the Cretaceous, the AFT data would still invoke denudation of several kilometres.

4.1.2. Southwestern Cape

AFT ages for 38 outcrop samples range between 86 ± 7 Ma (8832-66) and 163 ± 9 Ma (S-19) with stratigraphic ages being between Cambrian (Cape Granite samples) and Permian (Lower Beaufort Group samples). These samples were collected from sea-level to 1658 m and show no obvious correlation with age (Fig. 4). MTLs of >c. 13 μm were obtained for most samples, with TLDs being unimodal and modal lengths being between approximately 13 μm and 15 μm. Several samples have negatively skewed TLDs owing to

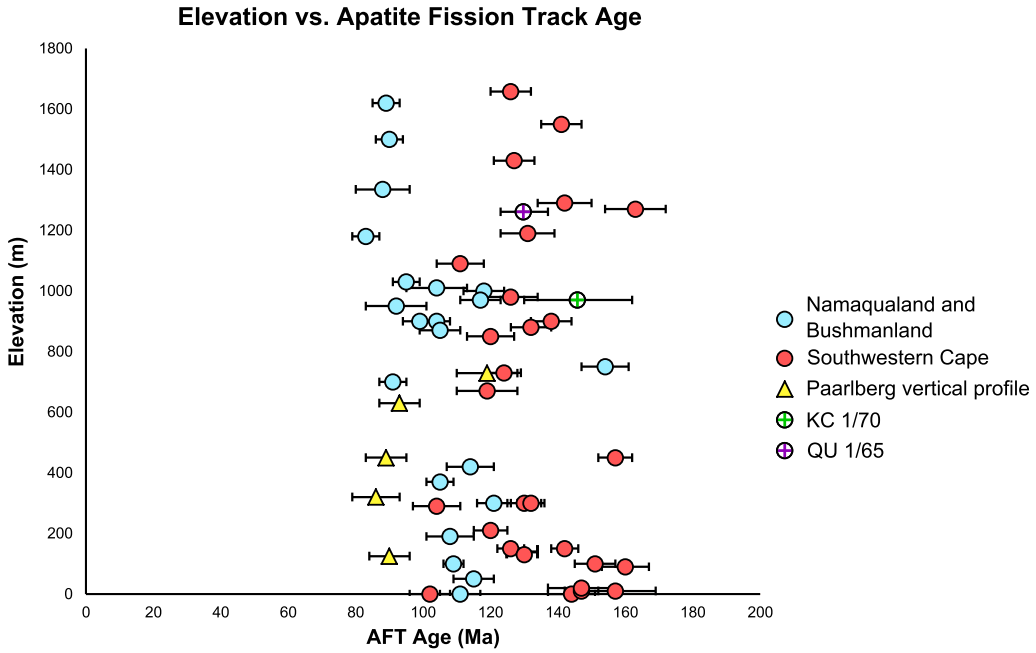

Fig. 4. Plot of AFT age against elevation. No clear trend can be identified in the regional data and, in fact, some of the youngest AFT ages are found at the highest elevations. Samples from the Namaqualand and Bushmanland region are generally younger than samples from the SW Cape particularly at high elevations. However, the Paarlberg vertical profile from the SW Cape records both the Late Cretaceous ages and a single Early Cretaceous age at the top of the profile. Data points for the two boreholes represent the AFT age–elevation point for the shallowest sample (see Fig. 7 for AFT age and MTL trends with borehole depth).

the preservation of varying proportions of highly annealed tracks within these samples (e.g., 8732-34, 8732-37 and 8732-40). The measured AFT ages for samples from the southwestern Cape are plotted against their MTLs (Fig. 5) and no simple correlation for these samples is observed. In general, these data suggest that maximum palaeotemperatures for most samples exceeded 110 ± 10 °C and that cooling from these elevated temperatures was initiated and largely completed by the end of the Cretaceous. The following discussion will, however, show that in detail the AFT data and thermal history models provide evidence for two discrete episodes of cooling: one during the Early Cretaceous (c. 140–120 Ma) and the other during the Late Cretaceous (c. 100–80 Ma).

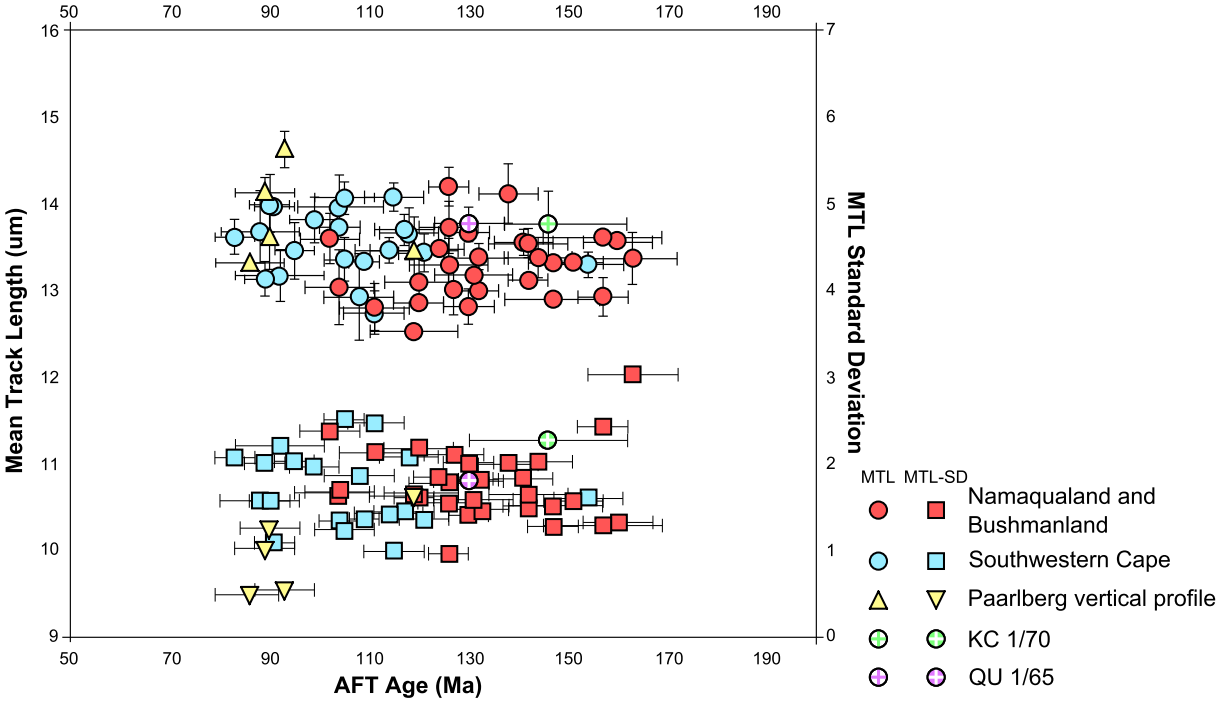

Fig. 5. Plot of AFT age against MTL (primary y-axis) and MTL standard deviation (secondary y-axis). No simple linear relationships for the regional dataset can be observed for either plot. The Paarlberg profile however shows a clear positive relationship between AFT age and MTL for the younger (i.e., c. 90 Ma), lower elevation samples while the older, Early Cretaceous age has a relatively short MTL with a larger MTL standard deviation. This could suggest that the uppermost sample has cooled during the early cretaceous but has undergone annealing at reasonably hot temperatures prior to exhumation of the lower part of the profile at c. 90 Ma.

The Early Cretaceous signal of cooling is recorded in samples at significant distances from the present day escarpment. At Verlatekloof, a vertical series of samples covering almost a kilometre in elevation show no significant age–elevation relationship. All the samples of fine-grained, feldspathic sandstone from the Permian, Lower Beaufort Group that constitute the Verlatekloof profile yielded Early Cretaceous AFT ages between 111 ± 14 Ma (8832-58) and 142 ± 16 Ma (8832-56), with MTLs varying from 12.81 ± 0.54 (8832-58) to 13.73 ± 0.60 μm (8832-54). The TLDs of these samples are all unimodal, with modal lengths generally between c. 13 and 14 μm and standard deviations between 2.13 and 1.47 μm. The measured distribution of single grain ages for most samples is consistent with those expected from age populations with a single mean age with $P(\chi^2) > 5$.

Additional evidence for the existence of two periods of cooling in the Cretaceous is provided by the AFT results from the vertical profile at Paarlberg (Fig. 4). Samples from Paarlberg yielded AFT ages of c. 90 Ma except for the uppermost sample which gave an older AFT age of 119 ± 18 Ma. The samples have relatively long MTLs and narrow, unimodal distributions. The uppermost sample, however, yields a slightly larger standard deviation owing to the preservation of a significant number of highly annealed tracks (< c. 10 μm). This sample also displays a much broader spread in single grain age, reflected by the much lower $P(\chi^2)$ value of 9.2% relative to the other samples which all have $P(\chi^2)$ values of 66%. The number of tracks measured in determining the MTL for the Paarlberg profile samples was small, varying between only 2 (for the shortest MTL of 13.32 ± 0.35 μm) and 35. The estimation of the true MTL must therefore be regarded as tentative.

Despite uncertainty arising from the scarcity of track length measurements, the AFT data and the variation of age versus elevation from the Paarlberg profile appears to indicate a discrete Late Cretaceous (c. 100–80 Ma) cooling episode. The lower four samples experienced palaeotemperatures greater than c. 110 ± 10 °C, whereas the uppermost sample experienced just less than c. 110 ± 10 °C, immediately prior to the initiation of accelerated cooling.

Cape granite outcrop samples from this region, which yielded AFT ages significantly older than c. 90 Ma, generally also have highly annealed tracks represented in their TLDs (e.g., samples 8732-35 and 8732-37). Like sample 8832-62 from the top of the Paarlberg profile, these older granite samples probably cooled from temperatures somewhat less than 110 ± 10 °C, and so fission tracks that accumulated prior to the proposed Late Cretaceous cooling episode would have been annealed during residence at elevated temperatures.

4.1.3. Borehole samples

Samples from borehole QU 1/65 yielded AFT ages which decrease systematically with depth from 130 ± 14 Ma at the surface to 11 ± 2 Ma at a depth of 2545 m, with MTLs also decreasing systematically from 13.78 ± 0.36 μm to 9.83 ± 0.84 μm, over the same depth range (Fig. 6). TLDs of the older samples (≥100 Ma) are all unimodal with modal lengths between c. 15 and 13 μm and standard deviations between 1.81 and 2.12 μm. All of these distributions contain a small proportion of highly annealed tracks. The presence of these shortened tracks is reflected by the reduced MTLs and relatively large standard deviations of c. 2 μm. The TLDs for the deeper samples (≥1900 m depth) have significantly wider standard deviations, between 2.56 and 3.63 μm. The deeper samples also have much wider distributions of single grain ages, relative to the shallower samples, with $P(\chi^2)$ values generally ≤5%.

The systematic decrease with depth of both apparent AFT age and MTL for the 11 samples from the QU 1/65 borehole is reminiscent of the progressive increase in the degree of thermal annealing expected from a borehole sequence currently experiencing maximum burial temperatures. However, the apparent AFT age at the top of this borehole is substantially younger than the stratigraphic age of their host rocks, indicating that samples must have experienced elevated palaeotemperatures in excess of 110 ± 10 °C. The range of measured

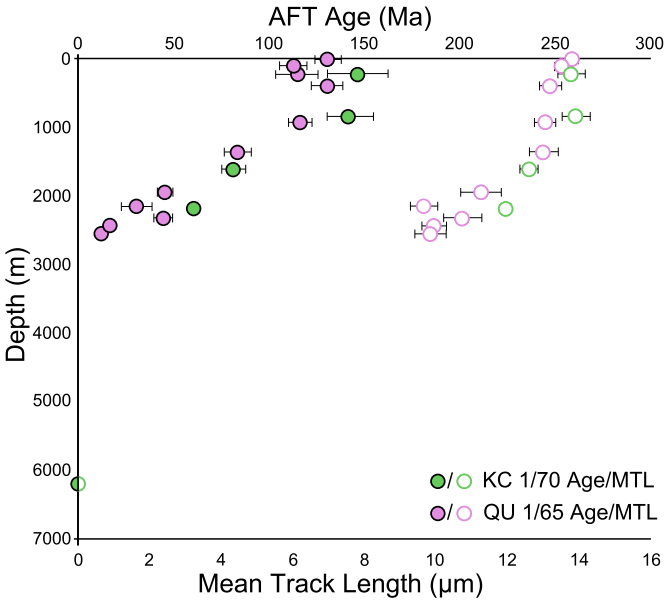

Fig. 6. Plot of MTL (primary x-axis) and AFT Age (secondary x-axis) against depth. Both Age and MTL mimic each other in their form. AFT ages are c. 120–150 Ma and MTL's are c. 13.5–14 μm in the upper 1–1.5 km before both profiles decrease with depth demonstrating the effect of the partial annealing zone. As no tracks were counted or measured in the deepest sample in the KC 1/70 borehole, a maximum depth for the base of the PAZ (i.e., Temp. = c. 110 ± 10 °C) can be estimated at c. 6 km.

AFT ages and MTLs suggests that cooling from the higher palaeotemperatures to near surface temperatures began, and was largely completed, during the Early Cretaceous. The pattern of decreasing AFT age and MTL with depth thus reflects post-Early Cretaceous thermal annealing. According to this interpretation, the pattern of annealing recorded by the QU 1/65 borehole samples should preserve important information on the maximum palaeogeothermal gradients attained since the Early Cretaceous.

Five samples analysed from borehole KC 1/70 yield AFT ages ranging from 146 ± 16 Ma at the top (222 m) decreasing progressively to zero at the bottom (6190 m) (Fig. 6). Assuming a present day geothermal gradient within the region is approximately 20 °C/km (Jones, 1987), the deepest sample is estimated to presently reside at a temperature of c. 140 °C and this is why no fission tracks are preserved within these samples. The two shallowest samples (KC-1 and KC-3) yielded similar AFT ages, 146 ± 16 and 142 ± 24 Ma respectively, both with relatively long MTLs of 13.77 ± 0.38 μm and 13.90 ± 0.39 μm. Despite their relatively long MTLs, samples from the KC-1/70 borehole have highly annealed tracks represented in their broad TLDs.

These data from borehole KC 1/70 suggest that the shallowest samples experienced Jurassic-Early Cretaceous maximum palaeotemperatures close to, but less than c. 110 ± 10 °C, and that cooling from these elevated temperatures was initiated during the Early Cretaceous. However, deeper samples, KC-6 and KC-8, yielded significantly younger AFT ages of 81 ± 12 Ma and 60 ± 6 Ma, respectively. If these deeper samples last cooled below 110 ± 10 °C during the Early Cretaceous then the observed AFT ages are not consistent with the degree of annealing expected at the relatively low present day temperatures of c. 52–64 °C.

4.2. Zircon fission track results

Zircon fission track (ZFT) analysis was performed on eight rocks from the Cape Granite suite in the southwestern Cape region. The upper and lower temperature limits defining the zircon partial annealing zone (PAZ) are more poorly defined than for AFT due to the accumulated radiation damage within zircon (Garver et al., 2005; Kasuya and Naeser, 1988). Estimates on the range of closure temperatures

governing fission track annealing in Zircon range from c. 180–300 °C (Gombosi et al., 2014; Rahn et al., 2004; Tagami and Shimada, 1996; Yamada et al., 1995, 2007) and therefore ZFT analysis provides insights into the timing of cooling through temperatures higher than possible with AFT analysis.

ZFT ages from this study range from 163 ± 10 to 437 ± 53 Ma. Apart from sample FTCG 31, all ZFT ages are significantly older than their sample equivalent AFT age and/or older than the nearest surrounding AFT age. Sample FTCG 31 provided the youngest ZFT age (163 ± 10 Ma) which overlaps within error of the nearest AFT age (8732-32: 156 ± 5 Ma). These two samples are both from the George Pluton of Cambrian age and are separated by c. 10 km. The overlapping AFT and ZFT ages imply that, locally, samples have cooled from a maximum palaeotemperature well above the AFT PAZ during the late Jurassic. This is attributed to km-scale denudation in response to the creation of syn-rift topography and the rapid lowering of base levels due to the opening of the South Atlantic.

More generally, ZFT ages are Permo-Triassic with the obvious exception of FTCG 06 which has a ZFT age of 437 ± 53 Ma. The Permo-Triassic ZFT ages are possibly linked to metamorphism associated with the development of the CFB during the Cape Orogeny (c. 220–290 Ma) (Frimmel et al., 2001; Tankard et al., 2009). Metamorphism at this time, however, is suggested to have been relatively low grade with metamorphic temperatures of c. 290–320 °C (Frimmel et al., 2001; Gresse et al., 1992). Fission tracks are therefore likely to be a population of younger tracks and partially annealed older tracks. The oldest ZFT age of 437 ± 53 Ma obtained from FTCG 06 likely reflects post intrusive cooling and indicates that this sample was not affected by metamorphism linked to the Cape Orogeny.

5. Thermal history modelling

5.1. Rationale and approach

The ultimate goal of low temperature thermochronometry (LTT) techniques is to derive quantitative thermal histories for samples and to use these to understand the surface and sub-surface processes that have produced the observed data. Inverse modelling of LTT data has become a popular method of generating numerical solutions for a rock's time–Temperature (t–T) history. Here we have used a Bayesian transdimensional approach to data inversion as described in detail by Gallagher (2012) and the multikinetic fission track annealing model of Ketcham et al. (2007) to derive robust thermal history information from the observed AFT data. Information on model parameters (i.e., range of temperature and times over which to search) is first provided to define a model space with a prior probability distribution, with an initial random model drawn within this space. The model space is then randomly sampled using a MCMC (Markov Chain Monte Carlo) approach (e.g., Gallagher et al., 2009; Gilks, 2005; Sambridge et al., 2006) whereby the current model is perturbed to produce a proposed model which is then accepted or rejected based on the likelihood probability of the model fitting the observed data. The novel aspect of this transdimensional approach is that the number of t–T points does not have to be defined explicitly and instead the data determine the complexity of the proposed thermal history model. The Bayesian aspect of the modelling technique penalises complex models proposed during sampling in favour of models with fewer t–T points that adequately fit the observed data. Using this iterative process of exploring the model space, many thermal histories are tested creating an expected thermal history weighted for its posterior probability distribution. A key advantage of this approach is that the outcome defines a range of allowable models and avoids highlighting overly complex, or 'spikey', thermal histories that may fit the data well but are unjustified based on the model and data uncertainties.

Predictions of how AFT age and TLDs evolve as a function of temperature and time are based on theoretical annealing models (e.g., Ketcham et al., 2007; Laslett et al., 1987). Recent work has shown that the initial length of fission tracks is significantly influenced by apatite composition (predominantly the relative proportions of Cl and F) (Carlson et al., 1999; Sobel and Seward, 2010) and that measurements of the kinetic parameter (Dpar) (e.g., Donelick et al., 2005; Ketcham et al., 2007) provide a good proxy for this compositional variability. Sample specific measurements of Dpar for modelled samples are unavailable because AFT analysis was completed prior to the common practice of measuring specific grain compositions (see Supplementary Material 2.1). Indications of the likely range of Dpar for the analysed samples were estimated from the apatite composition measurements determined by electron microprobe on the same Karoo sedimentary formations by Tinker et al. (2008a) and from Dpar measurements from basement lithologies by Kounov et al. (2009). These studies both showed that the apatite compositions from Karoo rocks and basement samples were comparable to the Durango Fluorapatite. To ensure that the compositional aspect of annealing was incorporated into the t–T models an initial 'standard' Dpar value of 2.04 ± 1.5 μm was assigned (approximate Dpar value of Durango apatite, Sobel and Seward, 2010) and the MCMC inversion was allowed to search for viable Dpar values within this range that were consistent with all the other observed parameters and stratigraphic constraints. A further advantage of allowing the kinetic parameter to be optimised within a specified range by the inversion scheme is that it allows for uncertainties that are not normally otherwise quantified, such as the uncertainty for initial track length (l_o) as a result of compositional variations, uncertainties in the annealing model parameters themselves, or other unknown factors.

Prior information on time and temperature was specified for the model space using t–T range for each sample where the prior information on time was simply the sample fission track age ± sample fission track age and the prior information on temperature range was set to 70 ± 70 °C. For basement samples, where an appropriate/effective stratigraphic age is unknown, a single constraint point was used with a time and temperature range 350 ± 10 Ma and 100 ± 100 °C, respectively. This constraint ensures that the thermal history is constrained at least as far back as the approximate age of Karoo deposition covering NMP basement rocks, but allows a large temperature range to be explored to allow the model to start at depth or at the surface if the data so requires it. Were an appropriate stratigraphic or emplacement age is known this is incorporated into the model as an added constraint. Aside from constraining the present-day temperature values to be 20 ± 10 °C no additional constraints were set. A selection of outcrop sample thermal histories that are representative of the entire data set are presented and discussed below. Thermal histories for all outcrop samples can be found in Supplementary Material 3.

Modelling of vertical and borehole samples was achieved by optimising an additional model parameter representing the temperature offset between the top and bottom sample. This temperature offset represents the effective geothermal gradient with temperature information being interpolated linearly through intermittent samples. Unfortunately, information necessary to evaluate palaeogeothermal gradients is sparse, particularly regarding Cretaceous thermal gradients in southern Africa. Present day geothermal gradients within the Karoo basin are also poorly constrained, with estimates ranging from 18 °C/km to 37 °C/km (Ballard and Pollack, 1987; Gough, 1963; Rowsell and Connan, 1979), and they are of course spatially variable. More detailed heat flow measurements in the Namaqualand and Bushmanland regions indicate a present mean surface heat flow of 61 ± 11 mW/m and geothermal gradients between 18 and 20 °C/km with a mean surface temperature of c. 20 °C (Jones, 1987). To allow for the uncertainty in geothermal gradient we set the range of possible values to be within 28 ± 10 °C/km.

The MCMC was run for c. 1,000,000 iterations after discarding an initial c. 100,000 iterations deemed to be "burn in" runs (Gallagher et al., 2009). The modelling results for 6 representative outcrop samples, one vertical profile and two borehole profiles are presented and discussed in detail in the following sections. Additional models for

other samples are available in the Supplementary material. The output of the Bayesian approach is a collation of all thermal history models that have been tested, each with an associated posterior probability. Therefore a summary probability distribution map of temperature at a given time (at intervals of 1 Myr) can be generated. From this collection of thermal histories a mean thermal history model (weighted for its posterior probability), termed the expected model, is determined with associated 95% credible intervals which provide the uncertainty on the inferred model. The nature of the expected model is that it will retain well constrained features (i.e., features common to many individual models) while more complex deviations observed in only a small number of models are averaged out. We believe that the expected model, and its associated probability, provides the most robust insight to the thermal history evolution.

For all outcrop models the predicted AFT ages and MTLs are within 3% of the observed values (i.e., predicted/observed = 0.97). The majority of borehole samples also show good agreement (i.e., predicted/observed > 0.9) with all predicted values within 26% of the observed data. Estimates of the kinetic parameter Dpar for out crop samples range from c. 1.6 to 4 μm but are predominantly between 2 and 3 μm. Most borehole samples also fall within this range but 8732-97 estimate of 5 μm. This seems an unusually large Dpar value however Dpar measurements have been shown to range from at least c. 1.5 to 5 μm (Carlson et al., 1999; Donelick et al., 1999; Sobel and Seward, 2010) and therefore the model predictions are deemed to be realistic. As initial Dpar values were estimates, preliminary models were run using larger and smaller initial values of Dpar with a smaller uncertainty on the estimate (See Supplementary Material 4). Adopting this approach typically resulted in a minor change to the maximum temperature recorded by the thermal history and a slight increase in age of the entire thermal history. The change in timing is minor and doesn't impact on our interpretations of the models. Moreover, the overall form of the thermal history is largely maintained.

5.2. Modelling results for Namaqualand and Bushmanland

A period of enhanced cooling is relatively well constrained for sample 8732-46, having begun between c. 170 and 150 Ma and continuing through the early Cretaceous (Fig. 7). Cooling becomes slightly more protracted through the middle to Late Cretaceous, but this second phase of cooling is less well constrained than the first. From the end of the Cretaceous until the present minimal additional cooling is inferred and the model is better constrained.

Cooling occurs slightly later for sample 8732-43, starting between 150 and 130 Ma (Fig. 7). For both of these samples cooling begins at similar temperatures c. 110 °C, but progresses at a slower rate through the PAZ for 8732-43 which is estimated to have cooled below 60 °C at c. 90 Ma. Unlike the relatively sharp transition between rapid and very slow or no cooling seen in the model for 8732-46, here the transition is smooth with the cooling rate estimated to have decreased steadily to the present day with less than 10 °C cooling since the Oligocene.

Both of these samples from this region record clear evidence for Early Cretaceous cooling, whereas the third sample, 8832-78, records a distinctly younger event (Fig. 7). For this sample the thermal history from the Permian through to Jurassic-Early Cretaceous is poorly constrained. However, a well resolved and rapid period of cooling through the PAZ is required at c. 100–90 Ma. Cooling continues at a lower rate through to early Eocene after which time there is minimal additional cooling indicated for this sample.

Fairly rapid cooling rates which then become more moderate over time as seen in samples 8732-46 and 8732-43 are more consistent with an initial phase of enhanced erosion which is then subdued rather than post magmatic cooling which would have a significantly faster cooling history. This period of denudation driven cooling is coeval with rifting of the South Atlantic margin and is likely a response of river incision to the newly created base level of the Atlantic Ocean. The slight differences in the timing and the rate at which cooling occurred for the different samples may be related to elevation differences (different initial structural depths); lateral retreat of the incising rivers; lithology of the eroding substrate or a combination of all these factors.

5.3. Modelling results for the Southwestern Cape

In the SW Cape region, sample 8732-36 is located 150 m above sea level on the coast and is a Cape Granite emplaced during the Cambrian. For this reason, the sample was assigned an initial t–T constraint of 300 ± 50 °C at 550 ± 50 Ma. The temperature at this time is largely irrelevant so long as it is hotter than c. 110 ± 10 °C and therefore all fission tracks are annealed at the time of emplacement. The sample yields an expected thermal history that implies rapid cooling at c. 150–140 Ma through to c. 115 Ma (Fig. 8). Before and after this very well defined cooling episode the thermal history is less well constrained. Despite this, the expected thermal history shows minimal cooling after c. 110 Ma.

Samples 8732-40 and 8732-54 are separated by 20 km and represent the top and bottom of a near vertical profile through the Verlatekloof (Fig. 8). Unlike basement samples, where the pre-Cretaceous history is essentially unknown, the stratigraphic age of these samples (Permian-Lower Beaufort Group) can be used to provide additional a priori thermal history information by constraining the temperature at this time to surface temperatures. Prior to this stratigraphic constraint the model is left unconstrained. Setting the model up in this way allows tracks which have formed before deposition of the sedimentary rock and have not been fully annealed over the samples thermal history to be preserved. Both samples yield expected thermal histories with enhanced cooling beginning at approximately the same time (c. 140–130 Ma) with the upper sample cooling slightly later than the lower sample. The manner of cooling, however, is distinctly different with 8732-54 showing rapid cooling between 140 and 110 Ma before more moderate to slow cooling from 50 Ma to present day, whereas 8732-40 exhibits a monotonic cooling history from 130 Ma to the present day.

5.4. Modelling results for vertical and borehole samples

The Paarlberg vertical profile consists of five granitic rocks collected over a range of elevations between 125 and 730 m and was constrained in the same manner as sample 8732-36 (see above). The expected thermal history produced for the Paarlberg vertical profile mimics the history of sample 8832-78 with an absence of any cooling prior to a sudden, rapid and well constrained cooling event (Fig. 9). This rapid cooling occurred at c. 100–90 Ma, with initial cooling possibly starting slightly earlier. By 70 Ma the rate of cooling had decreased significantly and by the early Eocene was negligible.

Using the estimate of the geothermal gradient described above, a present day temperature estimate is explicitly defined for each sample in both borehole profiles. Moreover, each sample is given a specific constraint reflecting their stratigraphic age. As the basement samples force the models to begin in the Proterozoic, the presence of inherited tracks in sedimentary rocks, that have not been fully annealed, will be dealt with during the modelling.

The KC1/70 model shows that three shallowest samples were at the surface in the Late Carboniferous to Permian and indicates burial to depths equivalent to a maximum palaeotemperature of c. 120 °C at c. 170–160 Ma (Fig. 9). During the Late Jurassic and Early Cretaceous monotonic cooling initiates and the sample progressively cools through the AFT PAZ until the early-Eocene (c. 50 Ma) where near surface temperatures were reached. Only minor, and not likely significant, heating of the samples occurs over the last 50 Ma bringing samples to their present day temperatures.

The same modelling approach as used for KC1/70 was adopted for QU1/65 borehole (Fig. 9). Like KC 1/70, the model indicates progressive

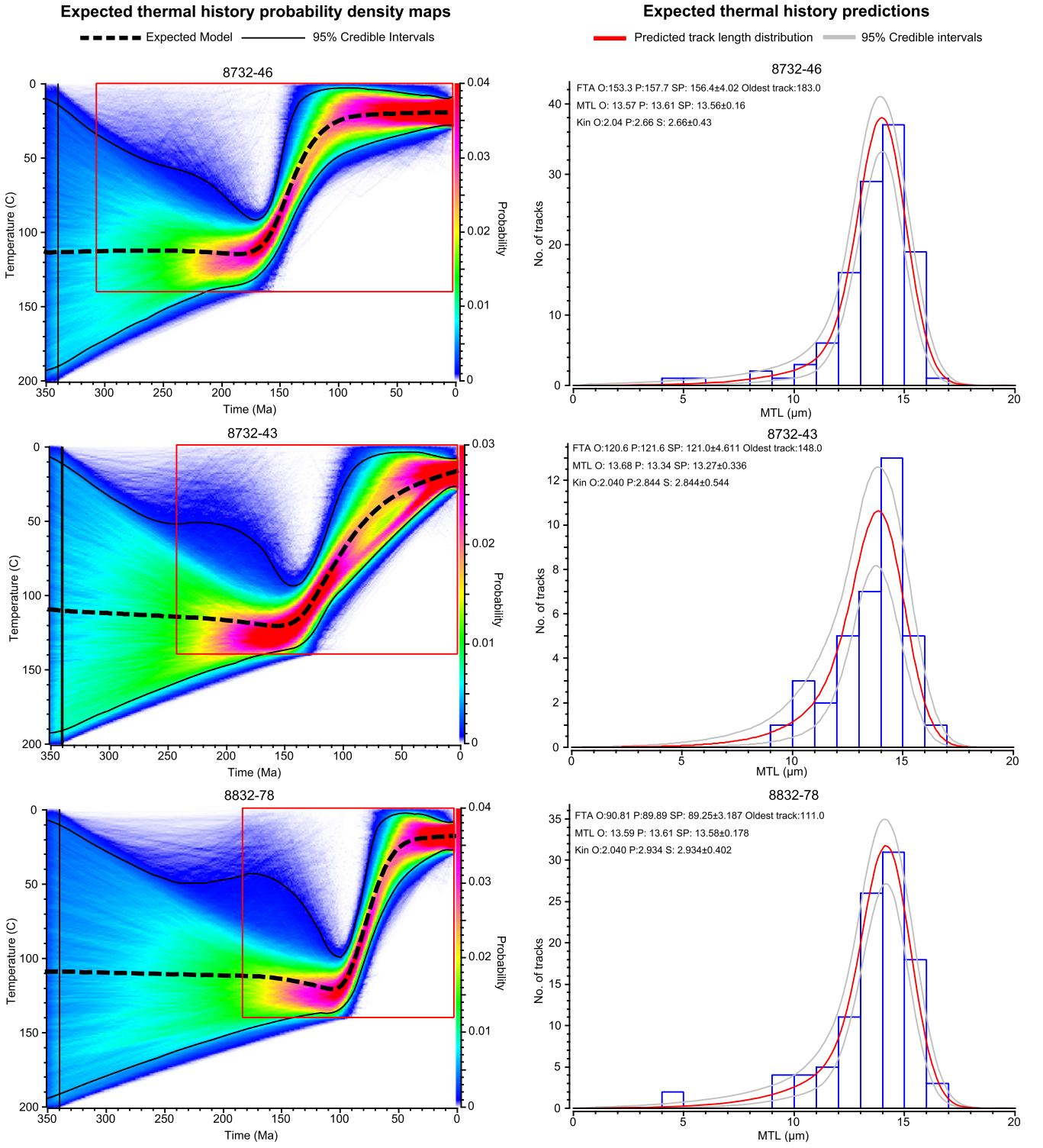

Fig. 7. Thermal history modelling results for three samples from the Namaqualand and Bushmanland region. From top to bottom models show: Fairly rapid cooling from c. 160–130 Ma; more protracted cooling through 150–90 Ma; and rapid cooling from 100 to 80 Ma. Left hand side plot: Dashed black line shows the expected model (i.e., average of all models weighted for their posterior probability); solid black lines indicate 95% credible intervals for the expected model; the colour map indicates the probability distribution of tested models at a resolution of 1 Myr. Red box indicates the prior information on temperature and time. Black box indicates an additional thermal history constraint. Right hand plot displays observed and predicted values of important AFT parameters; histogram shows the observed TLD; red curve indicates the predicted TLD, grey curves indicate 95% credible intervals (i.e., uncertainty) for TLD prediction. A constraint box with a large temperature range at the beginning of Karoo aged deposition confines the model to exploring younger thermal events while allowing the model freedom to start at the surface or at depth if the data so require.

burial from the last known stratigraphic constraint point (i.e., c. 260 Ma) until the upper sample was at a maximum palaeotemperature of c. 130–125 °C at 150–140 Ma. Cooling of c. 70 °C occurs from this maximum palaeotemperature over c. 50 Myr bringing the upper sample to temperatures of c. 50 °C by c. 90–80 Ma. This cooling episode was followed by a period thermal stability or potentially very slight reheating before cooling resumes at c. 70–50 Ma bringing the profile to its present day temperatures by the present day.

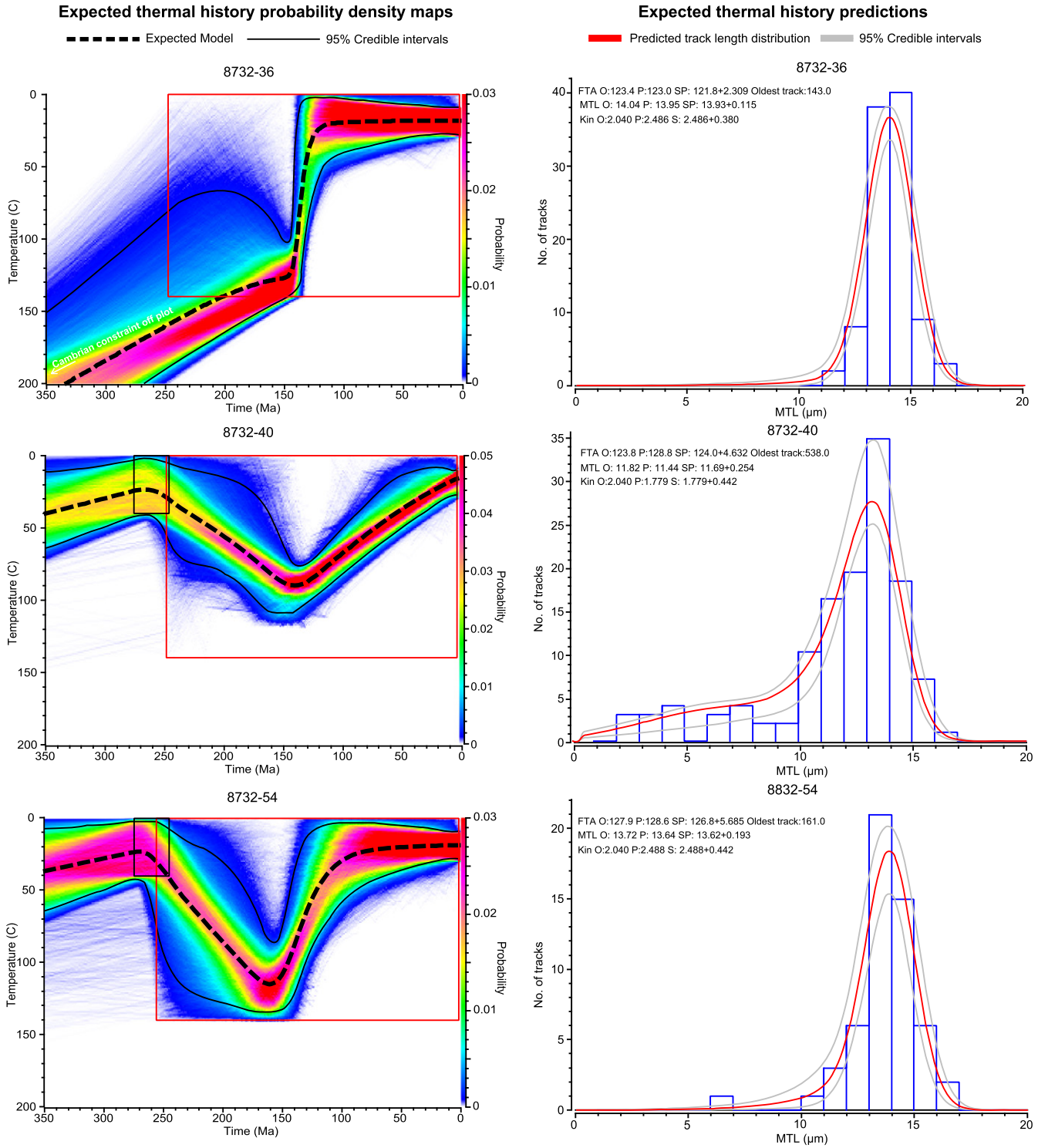

Fig. 8. Thermal history modelling results for three samples from the SW Cape region. From top to bottom models show: Very rapid cooling at c. 130–120 Ma; more protracted cooling initiating at c. 130 Ma; and fairly rapid cooling from 150 to 100 Ma. See Fig. 8 for legend. Constraint box used for samples 8732-40 and 8732-54 reflect their Permian Lower Beaufort Group stratigraphic age, prior to this the model was left unconstrained to allow for inherited tracks in sedimentary rocks. Sample 8732-36 is from a Cambrian Granite and therefore has been assigned a constraint to ensure that the sample was at temperatures well hotter than the base of the AFT partial annealing at c. 500 ± 50 Ma.

5.5. Summary of modelling results

Due to the sensitivity of the AFT method over the temperature range of the PAZ (c. 110–60 °C), cooling through this range provides the most robust constraints on cooling rates. The expected thermal histories, however, are accompanied by uncertainty characterised by the posterior probability distribution and therefore calculating precise cooling rates is unjustified and was not attempted. However, indicative estimates of the likely cooling rate of samples through the PAZ shows that most samples, including borehole profiles, for which cooling begun at c. 130 Ma did so at c. 1 to 2 °C/Ma. The thermal history for sample 8732-36 in contrast, is particularly well constrained and appears to

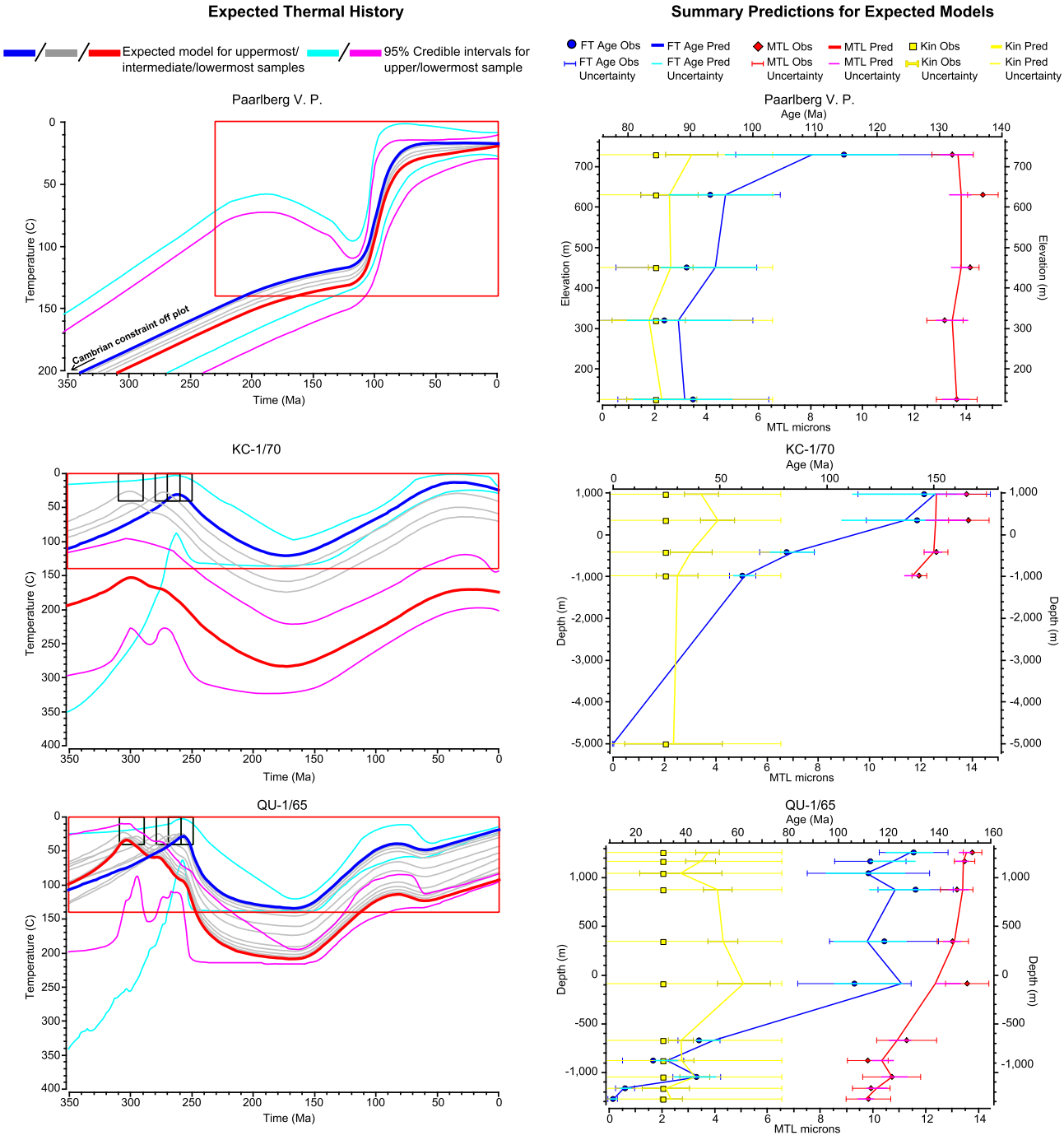

Fig. 9. Thermal history modelling results for two borehole profiles from the SW African plateau and one vertical profile from the SW Cape. From top to bottom models show: KC1/70 — protracted cooling initiating at c. 170–150 Ma through to c. 50 Ma. QU 1/65 — fairly rapid cooling from c. 150 Ma to 100 Ma prior to thermal stability or possibly slight reheating then a second phase of cooling is recorded at c. 60 Ma. Paarlberg VP — rapid cooling initiating at 100 Ma, note vertical profile samples initially have a temperature offset defined by the geothermal gradient but have the same present day temperature as they are all from rock exposures at the surface. Left hand side plot: Expected thermal histories for the profiles. The uppermost sample history is in dark blue with cyan 95% credible intervals, the lowermost sample is red with magenta 95% credible intervals, intermediate samples are grey. Central plot: Relationships between model predictions of AFT parameters (Dpar, AFT Age, MTL) and observed data with increasing profile depth. Details of symbology are on the figure.

have cooled much faster at c. 5 °C/Ma. Where cooling at c. 90 Ma is suggested (i.e., sample 8832-78 and Paarlberg vertical profile) the cooling appears to be fairly rapid and consistently on the order of 2–3 °C/Ma.

The models presented here and the additional models available in the Supplementary material can be broadly classified into groups showing enhanced cooling at two distinct periods: i) an older period between c. 150–130 Ma, and ii) a younger period between c. 100–80 Ma. The younger of these cooling events is typically observed to be more rapid, and of sufficient magnitude for samples to have cooled from depths where temperatures exceeded the upper limit of the PAZ (i.e., >110 °C). The earlier phase of cooling is represented by different styles of cooling ranging from rapid and short lived cooling for some samples followed by slow cooling through the Cenozoic, to slow, monotonic cooling from the initiation of cooling through to present day. This cooling event is broadly coeval with the period of rifting and continental break-up and we interpret it to be a result of denudation linked to

erosion, and potentially uplift, of rift flank related topography as well as to the formation of a new base level for rivers draining the interior. Variation in cooling patterns observed in individual samples could be due to the different responses of river incision with increasing distance from the rift margin or due to lithological variations and differences in erodability. The earliest cooling appears to be a regional event, albeit with different magnitudes and rates, rather than focused only at the coastal margins, as indicated by the syn-rift cooling recorded far inland (e.g., sample site 8732-40 and 8732-54) and the coherent pattern along the entire margin. The younger episode at c. 100–80 Ma, although seen in previous AFT studies across the southern (Tinker et al., 2008a), western (Kounov et al., 2009) and eastern margins (Brown et al., 2002), appears to be focused at localities within the SW Cape region that are controlled by differential displacement across significant normal faults. We suggest that this structural reactivation in places on normal faults along the western margin has caused the earlier thermal history record to be effectively removed by erosion.

6. Discussion

6.1. Timing and magnitude of denudation

Widespread Karoo magmatism occurred in the Mid Jurassic (c. 180 Ma) with only minor intrusive activity occurring across the interior plateau in the Early Cretaceous (Jourdan et al., 2005; Trumbull et al., 2007; Verwoerd and de Beer, 2006). As younger post-rift magmatism is limited to local, albeit numerous, kimberlite and alkaline intrusions c. 50–500 m in diameter (Cornelissen and Verwoerd, 1975), it is unlikely that there has been a regional thermal overprint on samples in this study. The AFT data obtained throughout the study area is therefore suggested to provide strong evidence for substantial denudation driven cooling of the crust during the Cretaceous. More specifically, the data indicate an initial Early Cretaceous cooling event associated with rifting and continental break-up which was followed by discrete cooling episodes during the Late Cretaceous.

One of the advantages of the joint inversion of the borehole profile data is that the expected thermal histories and 95% credible intervals can provide a robust estimate of the palaeogeothermal gradient with an upper and lower range. The models for KC 1/70 indicate an expected geothermal gradient of c. 22 °C/km with an upper limit value of 26 °C/km and lower limit of 18 °C/km (Fig. 9). The models for QU 1/65 indicate a wider range between 27 °C/km and 15 °C/km with the expected model predicting 22 °C/km (Fig. 9). Using these estimates of the palaeogeothermal gradient an estimate can be made of the amount of denudation associated with each cooling event predicted from thermal history modelling. Using the expected thermal history model and a value of 22 °C/km for the geothermal gradient it is estimated that, on average, the margin has experienced 4.5 km of denudation since the Late Jurassic–Early Cretaceous. Using the upper and lower estimates for the geothermal gradient, the amount of denudation then ranges from 3.7 to 6.6 km. The most extreme minimum and maximum estimates of denudation are 2.2 and 8.8 km, respectively, based on the upper and lower ranges of the geothermal gradient and possible thermal histories bounded by the 95% credible intervals. A summary of these calculations is provided in Supplementary Material 5.

6.2. The SW African LTT data set

The AFT data presented here complement previous AFT studies from the along the Orange River valley (Brown et al., 1990; de Wit, 1988) and across two transects through Namaqualand (Kounov et al., 2009) extending from the coastal plain to the inland plateau (Fig. 1). AFT ages presented by de Wit (1988) range between 70 and 129 Ma with MTLs between 13.16 and 14.23 μm and are interpreted to be the result of two thermal events. The first which is related to rifting (c. 120–130 Ma) and the second ascribed to a Late Cretaceous of alkaline magmatism in the Bushmanland plateau (c. 70 Ma). These younger ages are present far into the Bushmanland plateau with sample PTD-12 at an elevation of 900 m yielding an AFT age of 73 ± 4 Ma. Although numerous intrusions are documented over the Bushmanland plateau the closest reported intrusion to this sample is only c. 100–200 m in diameter (Smith, 1986) and is c. 60 km SW of the sample location. It is therefore deemed unlikely that the intrusion has had a significant thermal influence on this sample's cooling history. PTD-12 was collected c. 20 km East of the Hartbees River Thrust fault while sample S-21 from our data set was collected at a similar elevation (1010 m), only c. 10 km north of PTD-12 but 15 km west of this fault, and has an age of 104 ± 9 Ma. Reactivation of Pan-African shear zones in Central Namibia was documented by Raab et al. (2002) and Brown et al. (2014) and was attributed to compression along the Damara belt c. 70 Ma. It is therefore possible that the large variation (40 Ma) in AFT ages between PTD-12 and S-21 is a result of differential denudation over the major Hartbees River Thrust fault following reactivation at in the Late Cretaceous (c. 80–60 Ma) rather than linked to a thermal overprint related to intrusion.

Kounov et al. (2009) presented data from a NE trending transect from the coast to Pofadder and an approximately E–W transect further south from the coast to Williston on the plateau. Data from both transects document a period of cooling from 115 to 90 Ma ascribed to tectonic uplift of the margin. However, older AFT ages observed from the southern transect are suggested to represent an older, Late Jurassic–Early Cretaceous cooling event (160–138 Ma) which the authors relate to regional thermal relaxation following Karoo magmatic activity (c. 180 Ma). This earlier event overlaps with the first cooling episode advocated in our data (i.e., 150–130 Ma) which we suggest is mainly the result of the removal of syn-rift topography. An additional observation made from these data is the abrupt age variations over individual fault lineaments and the variable denudation occurring over individual fault blocks. The contribution of our new data to this complex area seems to highlight further the effects of tectonic disruption that this structurally complex area seems to have experienced with an age of 154 ± 7 Ma (8732-46) at an elevation of 750 m adjacent to ages of c. 90 Ma (e.g., 8832-78 and -79) at elevations of c. 1500 m (Fig. 10). For palaeogeothermal gradients close to that of present day values, this abrupt age variation cannot be ascribed to compositional differences and requires of km-scale variations in denudation across normal faults. The additional complexity of the basement structures and their relative uplift history is still unresolved in detail and will require additional sampling at a higher spatial resolution to be able to document individual fault block displacements.

A similar relationship is observed for the cross-section drawn between Cape Town and the QU 1/65 borehole location (Fig. 10) is roughly perpendicular to two major northwest trending normal fault systems: the Saldana–Franshoek fault zone and Piketberg–Wellington fault zone. The Worcester fault which has an estimated Late Jurassic-Early Cretaceous down-throw to the south of c. 6 km also trends NW–SE in this region (Dingle et al., 1983; Tankard et al., 2009) and it is across this lineament that the abrupt transition from Early to Late Cretaceous AFT ages occurs. AFT ages and TLDs for samples within each intervening structural block appear to be more uniform.

Although the Late Cretaceous episode of erosion, advocated in this study, is observed across the western and southern continental margin in discrete fault blocks it has been documented regional across southern Africa in previous thermochronometry studies. AFT data by Brown et al. (2000, 2002) document Late Cretaceous denudation of the Drakensberg Escarpment and similarly Tinker et al. (2008a) report a 100–80 Ma. Apatite (U–Th)/He (AHe) dating by Flowers and Schoene (2010) and Stanley et al. (2013) also document cooling at this time occurring well inland of the margin and on the plateau. The picture emerging for the Late Cretaceous in southern Africa therefore seems to include a regional,

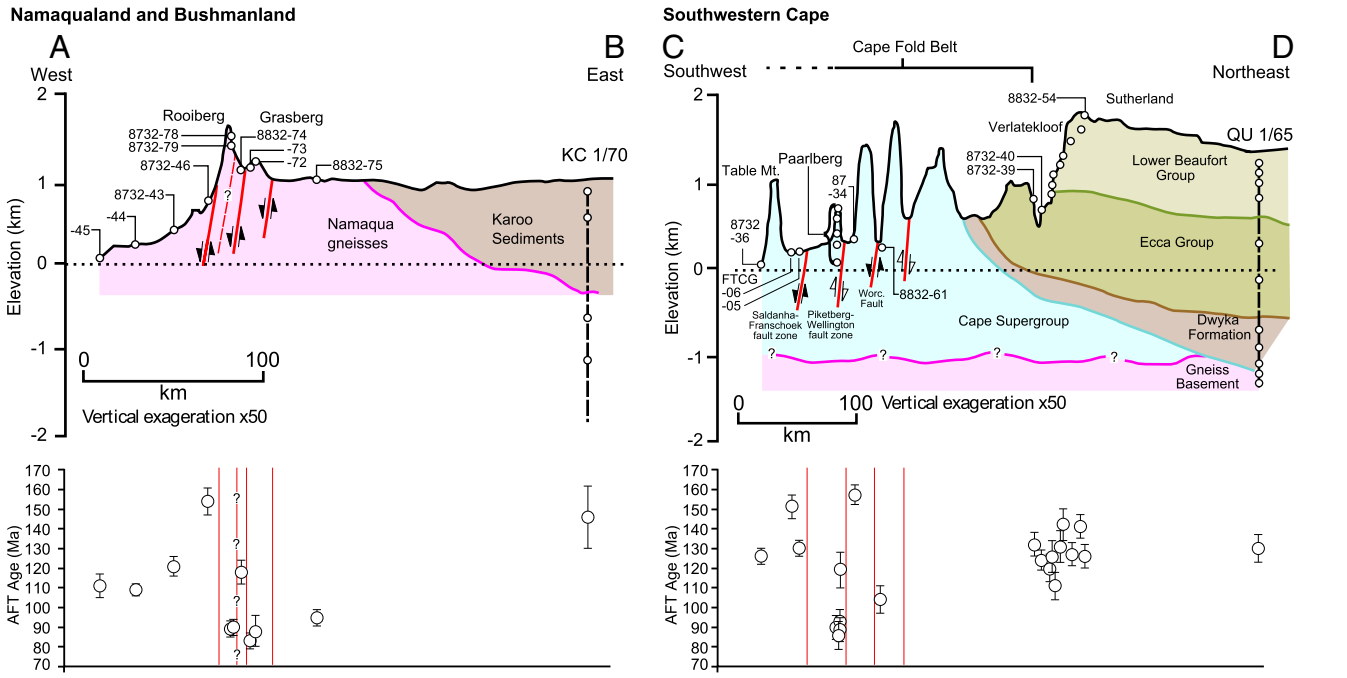

Fig. 10. Geological cross sections through the Namaqualand and SW Cape regions with projected AFT data (Note exaggerated topography, ×50, and different horizontal scales for each section). Sections highlight the offset in AFT age over individual fault blocks in both the Namaqualand and SW Cape regions.

sub-continental scale event which has been locally enhanced by discrete tectonic reactivation and inversion of fault structures (Fig. 12).

A consistent observation from AFT and AHe analyses in Southern Africa is that there is no signal of kilometre scale regional erosion during the Cenozoic. The current thermal history modelling indicates long-term average Cenozoic erosion rates of c. 5–10 m/Ma. This interpretation is consistent with shorter term (0.1–1 Ma) average estimates of erosion rates (0.5–4 m/Ma) for the study area and wider region based on cosmogenic isotope measurements (Cockburn et al., 2000; Decker et al., 2013; Kounov et al., 2007). These results do not support the hypothesis that the current South African topography postdates c. 30 Ma (e.g., Burke and Gunnell, 2008; Paul et al., 2014), with an earlier plateau having been eroded to a regional low elevation pediplain, as isostatic rebound at this length scale would require km scale (c. 4–5 km) denudation across the coastal plain at this time as well as much deeper levels of erosion than are calculated for the interior. This, however, is not to say that surface uplift has not occurred across south Africa but limits the total amount of erosion to less that 0.5 to 1 km which is in accordance with similar conclusions drawn from geomorphological analysis of the lower Orange catchment (e.g., Dauteuil et al., 2014).

6.3. Onshore Late Cretaceous-Cenozoic geological constraints

Independent terrestrial geological evidence that can be used to help constrain thermal history models is limited and poorly dated. However, the preservation of fossiliferous crater facies and crater infill sediments observed at kimberlite and melilitite intrusive bodies within the SW Cape and Namaqualand region (De Wit, 1999; Smith, 1986; Viola et al., 2012) implies that very little post emplacement erosion has occurred at these sites (less than a few 100 m). This includes Late Cretaceous–Early Tertiary fossil frogs in pipes from the Gamoep cluster (Haughton, 1931); Late Cretaceous petrified fish, frogs and insect wings from a kimberlite crater at Stompoor (Smith, 1986) and Late Cretaceous crater lake fossilised frogs in Marydale (Trueb et al., 2005) and dinosaur remains found near Kangnas (de Wit et al., 1992).

Near Banke Farm, south of Vaalputs silicified and kaolinitised conglomerate and coarse grained, cross-bedded sandstones form prominent mesas and inliers (Brandt et al., 2003). Brandt et al. (2005) describe additional sedimentary deposits of from the Vaalputs and Santab-se-Vloer Basin that overly the Dasdap sequence. Rounded pebbles of various compositions within the conglomerate horizons and the occurrence of widespread cross laminations in the Dasdap sediments suggest that these sediments were deposited in a fluvial (alluvial fan) environment. The dominant presence of granitoid and blue-vein quartz pebbles in conglomerate units suggests a metamorphic basement source. However, occasional pebbles of Dwyka tillite composition, confined to the Vaalputs sequence, were also described by Brandt et al. (2005). The composition of conglomerate clasts, palaeocurrent indicators and grain size characteristics indicates a westerly provenance and easterly directed palaeocurrents for the Dasdap and Vaalputs sediments (Brandt et al., 2003, 2005). In places, the Vaalputs sediments overly Late Cretaceous melilitite pipes and, in others, the Dasdap sediments. An upper age limit of c. 67 Ma for these sequences is suggested (Brandt et al., 2003, 2005; Viola et al., 2012). The similarities between lacustrine deposits (Scholtz, 1985) and those observed in the Dasdap and Vaalputs sequence also support the suggestion of a post-Cretaceous age for these deposits but their age and therefore their wider geological significance is still largely uncertain. However, the history and pattern of erosion documented here from the onshore AFT data would be difficult to reconcile with an earlier age for the Dasdap sequence, given that major (km scale) erosion is indicated for the Early Cretaceous in this region.

The Vaalputs and Santab-se-Vloer basins are intersected and bounded by prominent NNW–SSW trending faults, and one particular group of outcrops of Dasdap sediments at Kookoppe form a fault bounded, north-northwest linear chain. This is in keeping with the predominantly NNW–SSE structural trend observed within the wider region (Viola et al., 2012). The highland region of Namaqualand, composed of crystalline basement rocks, is characterised by prominent structural lineaments that are readily identifiable from satellite imagery (Kounov et al., 2009; Viola et al., 2012). In the absence of well dated stratigraphic markers, Viola et al. (2012) and Salomon et al. (in press) have documented a range of field evidence from the Namaqualand highlands and western Namibia, respectively, including small scale fault offsets,

discontinuities and slickenlines to derive a series of palaeo stress tensors. Based on their apparent correlation with African plate tectonic episodes it is suggested that these structures record multiple discrete phases of reactivation from the Pre-Cambrian to present. Despite disagreement between the two studies on the evidence for Santonian–Maastrichtian compression, both suggest phases of extension at c. 110–80 Ma. This extension may have been punctuated by local compressional events which only inverted suitably orientated structures.

These observations have two main implications in the context of this paper: i) erosion of basement rocks and Dwyka units occurred during the Cretaceous, possibly related to tectonically steepened river gradients and increased rainfall associated with the humid Late Cretaceous climate (Brandt et al., 2005; Partridge and Maud, 1987); ii) tectonic activity across the margin, including significant displacement and differential uplift across faults, extended inland for at least 150 km from the initial locus of rifting and certainly inland of the escarpment zone, and has been episodically active long after the initial phase of lithospheric extension and rupture.

6.4. The offshore sedimentary record

The offshore Orange and Outeniqua basins of South Africa's western and southern margins, respectively, are characterised by faulted syn-rift (Late Jurassic-Early Cretaceous) sequences unconformably overlain by thick Cretaceous post-rift deposits (Broad et al., 2012; Brown et al., 1995; Jungslager, 1999; McMillan, 2003; Paton et al., 2008; Rouby et al., 2009). The volumetric record of post-rift sediment influx to the western margin basin records two major peaks of over 10×10^{14} m^3 from 150 to 130 Ma and c. 11×10^{14} m^3 between 93.5 and 84.8 Ma with a significantly smaller contribution during the Cenozoic (5×10^{14} m^3) (Fig. 11a) (Guillocheau et al., 2012; Rouby et al., 2009). The earlier peak in sediment flux we believe reflects the erosional response to the rift stage of margin development (e.g., Brown et al., 2000; Rouby et al., 2009). The thickness of post-drift Cretaceous sedimentary units varies significantly along the length of the margin (McMillan, 2003); however, deposition appears to be coherent along all sectors of the margin until the late Cenomanian-early Turonian. This phase of deposition is characterised by a regional and well developed unconformity, 15At1–16At1 (c. 93–90 Ma) (Fig. 11b) (Hirsch et al., 2010; Kuhlmann et al., 2010; McMillan, 2003; Paton et al., 2008) and is interpreted to represent rejuvenated regional uplift and the onset of accelerated erosion of the margin.

Subsequent sediment accumulation within the offshore basins seems to be much less coherent with different sectors experiencing subsidence while others experienced uplift and erosion (e.g., McMillan, 2003) suggesting a more dominant and geographically variable local tectonic influence. Detailed seismic reflection data from the southern offshore basins have indeed provided evidence of discrete episodes of basin inversion and/or reactivation (Bate and Malan, 1992; Boyd et al., 2011; Hartwig et al., 2012; Paton et al., 2008; Tinker et al., 2008b; Van der Merwe and Fouche, 1992). In the Orange Basin inversion structures at the distal margin and normal fault displacement at the proximal margin in Late Cretaceous packages have been attributed to gravitational tectonics (de Vera et al., 2010). Uplift of the adjacent continent has been cited as a possible trigger for this tectonic activity in the offshore. Younger neotectonic inversion structures have been documented by Viola et al. (2005) which have been linked to the onshore structural network in southern Namibia and Namaqualand.

A second widespread unconformity marks late Maastrichtian-early Palaeocene (22At1, Fig. 11b) and a very significant reduction in the clastic input to the offshore basins of South Africa (McMillan, 2003). This observation is consistent with evidence from thermochronology and cosmogenic nuclide data as well as geomorphological analysis (Dauteuil et al., 2014) which all indicate very limited (<1 km) Tertiary erosion within the SW Cape and Namaqualand region. The distribution of sediment volumes, the presence of widespread unconformities offshore, coarse clastic deposits in the proximal sedimentary sequences and clearly documented inversion structures on at least some basin bounding faults within the southern margin (e.g., Bate and Malan, 1992) and Bredasdorp basins (Van der Merwe and Fouche, 1992) we believe provide a compelling case for episodes of inversion and related accelerated denudation affecting the hinterland of the continental margin (e.g., Guillocheau et al., 2012; Rouby et al., 2009; Tinker et al., 2008b).

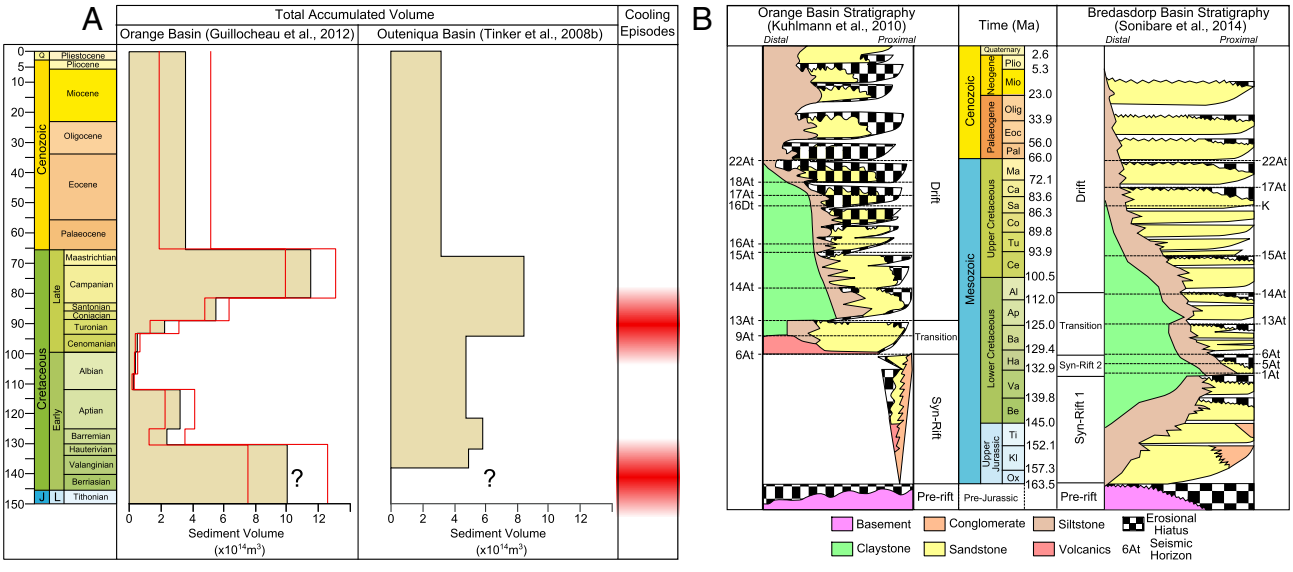

Fig. 11. Summary of offshore sedimentation history along the SW and S African margin. (a) Histogram of sediment accumulation in the Orange (after Guillocheau et al., 2012) and Outeniqua Basin (after Tinker et al., 2008b). Orange Basin accumulation shows two major peaks in accumulated volume from c. 150–130 Ma and c. 85–65 Ma. The latter of these peaks however, begins to develop in stages beginning at c. 90 Ma. A minor peak is also documented at c. 120–115 Ma. Outeniqua Basin shows two peaks in accumulated volume at c. 130–115 Ma and a second, more prolonged, period of accumulation from c. 90–70 Ma. Enhanced accumulation rates tend to correlate well with periods of enhanced accumulation (see Guillocheau et al., 2012 and Tinker et al., 2008b for details). (b) The two stratigraphic profiles representative of the Orange Basin (western margin) and the Bredasdorp Basin (southern margin).

The syn-rift unit is dominated by the presence of seaward dipping reflectors interpreted as large volumes of sub-aerial flood basalt volcanism synchronous with the initial extension of the lithosphere (Hirsch et al., 2009). Coarse continental clastic and fluvial syn-rift sediments were deposited in fault-bounded graben and half-graben during initial rifting and subsidence of the margin in the Late Jurassic/Early Cretaceous (Broad et al., 2012; Brown et al., 1995; Jungslager, 1999). The first drift succession forms a ramp-like unconformity with the underlying syn-rift sedimentary units and marks the rift to drift transition (1At1–6At1 around 130 Ma, Fig. 11) (Broad et al., 2012). The sediments are predominantly marine sandstone and shales and fluvial red beds (Broad et al., 2012; Gerrard and Smith, 1982; Kuhlmann et al., 2010). The Early Aptian to Late Maastrichtian sediments are deposited on the 13At1 and 14At1 unconformity in the Orange and Outinequa Basins, respectively, and define the transition to full marine conditions of the margin (Hirsch et al., 2010; McMillan, 2003; Muntingh and Brown, 1993). The sediments are predominantly fluvial–deltaic sandstones interbedded with clays and shales that were deposition in the middle shelf due to major progradation of the shelf (Broad et al., 2012; Brown et al., 1995; de Vera et al., 2010; Dingle and Robson, 1992; Hirsch et al., 2010). These units are the last fluvially influenced Cretaceous sedimentary deposits (McMillan, 2003; Paton et al., 2008; Van der Spuy, 2003). In the Orange Basin, the maximum thickness of sediments accumulated during the Cenozoic is c. 1200 m over the outer shelf and only a few hundred metres on the inner shelf (Hirsch et al., 2010). These sedimentary units are comprised of Lower Cenozoic sandstones and claystones and Oligocene–Early Miocene Carbonate sequences that were eroded during periods of intervening sea-level regression and/or localised tectonic instability of the margin (de Vera et al., 2010; Gerrard and Smith, 1982; McMillan, 2003; Wigley and Compton, 2006).

The chronology of the inferred denudational episodes documented in this paper is consistent with the detail of the depositional stratigraphy and architecture and with the overall sediment volumes recorded within the offshore Orange and Outeniqua basins (Fig. 11a) (Guillocheau et al., 2012; McMillan, 2003; Rouby et al., 2009; Sonibare et al., 2015; Tinker et al., 2008b). A recent compilation by Guillocheau et al. (2012) of sedimentary accumulation in the Orange and Walvis Basins documents a distinct phase of accumulation during the Late Cretaceous (93–65 Ma) separated from a high accumulation rate in the Early Cretaceous (136–112 Ma) by period of low accumulation (Fig. 11a). Isopach maps and well data in the Bredasdorp Basin, offshore to the south of the SW Cape, also indicate periods of enhanced sediment accumulation that are broadly coeval with the offshore record of the western margin of South Africa (Figs. 3, 11). Tinker et al. (2008b) demonstrated a similarly bimodal history with the highest rates and volume of sediment accumulation occurring during the Early Cretaceous (c. 136–130 Ma) and Late Cretaceous (c. 93–67 Ma). Complimentary AFT data presented by Tinker et al. (2008a) from the onshore margin of this region shows that two periods of enhanced denudation (c. 140–120 Ma) and (c. 100–80 Ma) correlate well with the timing of erosion inferred here and with the enhanced accumulation in the offshore basin.

6.5. Regional tectonic driving mechanisms

Both cooling episodes advocated in this study appear to have a regional footprint, extending well inland from the coast and into the elevated interior. However, in detail, the spatial pattern of AFT ages and thermal histories from the SW Cape indicate that although the Late Cretaceous event was expressed regionally across southern Africa it is also manifest in Namaqualand and the SW Cape by discrete tectonic inversion and km-scale differential erosion across major normal faults. This is consistent with recent theoretical thermo-mechanical models of rift formation that indicate the formation of brittle faults well inland (>100 km) of the locus of maximum extension and subsidence (Huismans and Beaumont, 2008; Huismans and Beaumont, 2011; Lundin and Doré, 2011).

The early phase of erosion we believe is in direct response to the onset of rifting and formation of the nascent South Atlantic Ocean. This erosional response was likely triggered by a combination of long wavelength (over c. 100's of km's) rift flank uplift (e.g., Rouby et al., 2013) as well as the establishment of a lower sea level, and therefore base level, for the major rivers draining the sub-continent (e.g., de Wit, 1999). The upper age limit for the onset of this cooling event is poorly defined as the thermal history begins when the sample cools below the base of PAZ which in this case occurs at c. 150–130 Ma. The upper age limit for the onset of this cooling event is poorly defined as the thermal history recorded by the AFT data begins when the sample cools below the base of PAZ which in this case occurs at c. 150–130 Ma. It is possible that exhumation of the sample started before this time, more closely tied to the Mid-Jurassic onset of rifting. If this were the case though the amount of erosion would be greater, and given the fairly good correlation between the predicted and observed sediment volumes for the west coast margin (Guillocheau et al., 2012; Rouby et al., 2009) any earlier erosion, if it occurred, must be relatively small. But we cannot discount this entirely and an earlier onset of erosion, i.e., at c. 165 Ma, is certainly possible.

Thermal histories that begin in Late Jurassic–Early Cretaceous typically show that cooling continues throughout the Barremian to Albian (i.e., c. 130–110 Ma). This relatively protracted period of enhanced erosion likely reflects modest rates of erosion (0.05 km/Ma) coupled with the isostatic response to erosional unloading which would have maintained elevated topography and enhanced erosion rates. Accumulated sediment volumes in the Orange Basin seem to support the addition of considerable volumes of sediment during the Barremian–Albian but less than the accumulated volume during the earlier syn-rift indicating a waning of erosion with reduction of relief.

The significance of the regional nature of the younger episode of erosion, and especially its extension well into the elevated interior of southern Africa, require further investigation but is consistent with the findings of other workers (e.g., Flowers and Schoene, 2010; Stanley et al., 2013) who proposed that the younger, middle to Late Cretaceous episode of erosion is likely to have been linked to regional dynamic uplift of the sub-continent (e.g., Forte et al., 2010; Gurnis et al., 2000). In this regard the recent theoretical work of Braun et al. (2013) is particularly relevant in that they have argued that, contrary to conventional thinking, low amplitude, continental scale dynamically supported uplift can trigger an erosional response that is temporally and spatially correlated with the phase of uplift. The key to establishing this response seems to require that major continental catchments are established, or evolve quickly, and increase in size proportional to the area of uplift. The increased size of the catchments draining the continent compensates for the moderate slope increase in the channel and ensures that a significant erosional response to long-wavelength uplift. In southern Africa this is almost certainly the case given that the proto Orange catchment which extends across the subcontinent was well established and linked to sea level by the base Late Cretaceous (de Wit, 1999; Dingle and Hendry, 1984).

However, on a more local scale, within the SW Cape and Namaqualand, this event is also expressed by discrete tectonic inversion and significant differential displacement and erosion across major faults. These episodes of tectonic reactivation (both inversion/renewed extension) are also expressed within the offshore basins in seismic reflection data. Specifically, Mid-Albian (and older) positive inversion structures are documented within the Bredsdorp basin (Van der Merwe and Fouche, 1992, their Fig. 9) and intense faulting and formation of growth- and roll-over structures, and evidence of uplift and truncation of the proximal basin affecting all pre Upper Cretaceous rocks, is beautifully documented within the Orange basin (e.g., Broad et al., 2012; de Vera et al., 2010; Hartwig et al., 2012; Paton et al., 2008). These offshore seismic data and the spatial and temporal pattern of offshore sediment

accumulation, coupled with our new onshore thermochronometry data, indicate a consistent history of active tectonic reactivation during the Late Cretaceous along of the SW Cape margins.

It seems clear that the expression of this Late Cretaceous tectonism varied spatially and temporally along and across the offshore margin, with positive inversion structures (e.g., Bredasdorp basin) occurring simultaneously with extensional faulting elsewhere (e.g., Orange basin). This variation is also seen in the pattern of erosion and inversion documented by our new AFT data onshore. On a regional scale, considering the offshore evidence, the geology of the remnant Jurassic-Cretaceous basins, gravity and magnetic anomalies and the onshore thermochronometry data collectively, we suggest that erosion following this period of inversion affecting the SW Cape has largely removed an earlier syn-rift half-graben basin, which we call the Malmesbury basin, illustrated schematically in Fig. 12. This basin we believe would have formed the westerly continuation of the series of such basins still preserved along the southern margin (i.e., Worcester, Swellendam, Heidelberg and Oudtshoorn basins). Clearly we cannot know the detailed geometry or structure of this inferred basin, and specifically it is likely to have been discontinuous, and possibly even segmented, especially where it crosses the complex region of the CFB syntaxis into the Bredasdorp basin towards the SE. However, the pattern of erosion and inversion documented onshore within the SW Cape by our new AFT and ZFT data coupled with the clear regional NW–SE structural grain seen in the gravity and magnetic anomalies for this region (see Supplementary data) does lend support for this idea.

The opportunistic exploitation of pre-existing structures where they were in a suitable orientation seems to have operated both during the formation of the narrow half-graben basins along the southern and western margins (e.g., Paton, 2006; Paton and Underhill, 2004; Paton et al., 2006) and during their subsequent inversion during the Late Cretaceous (e.g., 2; Bate and Malan, 199; Thomson, 1999). The plate

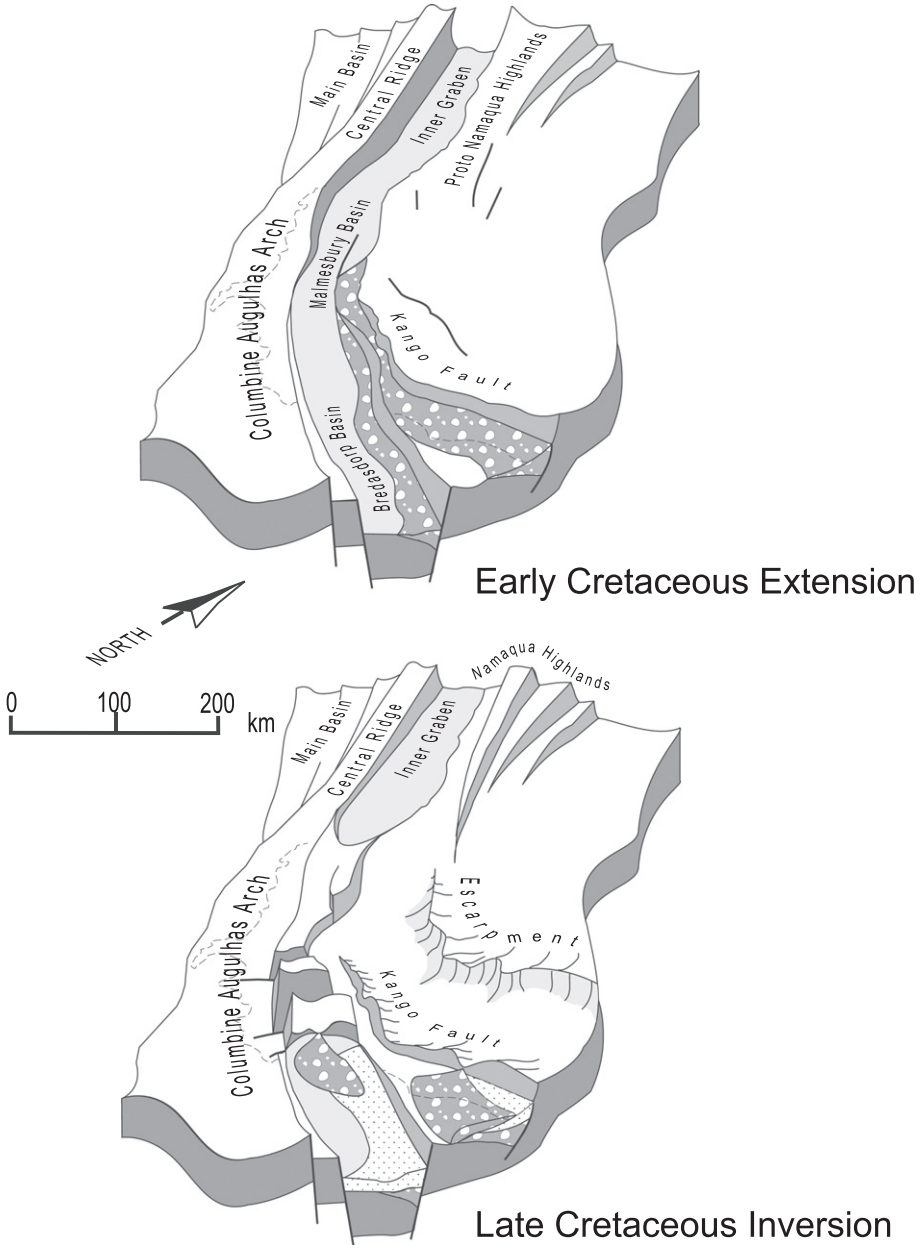

Fig. 12. Schematic illustration of the structural evolution of the SW Cape during the Cretaceous. Upper image portrays the early development of the Namaqua Highlands and major sedimentary basins through extension during continental rifting in the Early Cretaceous. In the lower image, river incision has carved out the prominent escarpment inland, while a regional tectonic inversion during the Late Cretaceous causes major fault block uplift within syn-rift basins.

kinematics and the spreading geometry south of the Agulhas Fracture Zone involved complex micro-plate rotations and ridge jumps during the early opening of the South Atlantic (Ben-Avraham et al., 1993, 1995, 1997) and culminated with the Falkland Plateau clearing the SW Cape during the Late Cretaceous (Fig. 3) and the Bouvet triple junction being located immediately south of the FAFZ and aligned almost exactly with the SW Cape at c. 94 Ma. The oceanic Aghulas Plateau (Parsiegla et al., 2008; Uenzelmann-Neben et al., 1999) was also formed at approximately this time by voluminous basaltic volcanism at c. 94 ± 5 Ma (Ben-Avraham et al., 1995; Martin and Hartnady, 1986). We suggest that this inversion style is more prevalent across the SW Cape than currently recognised elsewhere in southern Africa because the regional vertical stresses arising within the mantle were augmented by more locally focused lateral stresses arising from the tectonic geometry. While the exact timing, and detailed geometry, of these events depends on specifics of plate reconstruction models, and direct confirmation of the age of Agulhas Plateau magmatism is still outstanding, the broad coincidence in the timing of key events along the FAFZ points to a tectonic crescendo focused on this region during the Late Cretaceous.

Our primary conclusion that NW–SE and NNW–SSE oriented structures were tectonically reactivated resulting in km-scale displacement and differential erosion is compatible with palaeo-stress models for SW Africa at this time (Bird et al, 2006; Gaina et al., 2013) that indicate E–W directed compression along the SW margin, and with the inferred palaeo-stress tensors determined from field observations by Viola et al. (2012). Our results provide independent support for the inferences made by Viola et al. (2012) concerning the timing of tectonic reactivation of faults within Namaqualand during the Late Cretaceous. Interestingly, in this context, seismic analysis of the Ceres earthquake (29 Sep, 1969) located within the SW Cape, the largest recorded earthquake in South Africa (magnitude 6.2), indicates shallow, strike–slip displacement on a near vertical fault plane associated with the regional Worcester fault (Green and Bloch, 1971; Krüger and Scherbaum, 2014).

7. Conclusions

The data presented in this paper has significant implications for our understanding of the western continental margin of South Africa which has long been considered a 'passive' continental margin. These AFT data and thermal history models indicate that c. 3 to 5 km of denudation has occurred across the continental margin, extending inland across the escarpment zone onto the interior plateau. In detail the pattern of denudation is both spatially and temporally variable and includes evidence for at least two discrete episodes of enhanced erosion. The earliest related to the initial rifting and breakup of the margin during the Early Cretaceous and a later phase during Late Cretaceous, long after the initial rifting and break-up event.

Specifically we advocate that the following key geological events occurred:

i) Topography created during the early stages of continental rifting was progressively eroded causing up to 5 km of material to be denuded from the continent during the early Cretaceous (c. 150–130 Ma) and deposited in offshore syn-rift basins. Due to the major drop in base level during the opening of the Atlantic, the erosional response is has been transmitted into the continental interior via the Orange river catchment as well as being locally focused where up-thrown blocks occurred on the rift-flank faults.
ii) A combination of in plane stresses, propagating through the lithosphere and caused by relative plate motions, and vertical forces from an underlying buoyant mantle promoted a Late Cretaceous (c. 100–80 Ma), long-wavelength uplift of southern Africa which is also locally expressed by tectonic reactivation and inversion occurring at pre-existing structural discontinuities.
iii) The new AFT data and thermal modelling results do not provide any evidence of significant (km scale) regional denudation across this segment of the margin during the Cenozoic. However, these results do not exclude the possibility of surface uplift with only minor (< c. 0.5–1 km) and local enhanced erosion over this time.

Mapping the detailed spatial and temporal distribution of this Late Cretaceous tectonic episode (c. 100–80 Ma), and in particular resolving between it and discrete, latest Cretaceous/Early Cenozoic displacements and events (e.g., Brown et al., 2014; Raab et al., 2002, 2005) within the region, will require more detailed sampling and, ideally, the joint application of lower temperature apatite (U–Th)/He thermochronometry with apatite fission track analysis.

Supplementary data to this article can be found online at http://dx.doi.org/10.1016/j.tecto.2015.04.012.

Acknowledgements

This work has benefited from numerous discussions at various stages with Maarten de Wit, Chris Hartnady, Brian Bluck and Mike de Wit and we thank them for their generous input. We also thank Kerry Gallagher for his willing advice and assistance with thermal history inversion modelling. This work received logistic support from De Beers Consolidated Mines Ltd. which is gratefully acknowledged and was supported by the Natural Environment Research Council, UK by grant number NE/H008276/1.

References

Almeida, J., Dios, F., Mohriak, W.U., Valeriano, C.D.M., Heilbron, M., Eirado, L.G., Tomazzoli, E., 2013. Pre-rift tectonic scenario of the Eo-Cretaceous Gondwana break-up along SE Brazil–SW Africa: insights from tholeiitic mafic dyke swarms. Geol. Soc. Lond. Spec. Publ. 369 (1), 11–40.
Andreoli, M.A.G., Doucouré, M., Van Bever Donker, J., Brandt, D., Andersen, N.J.B., 1996. Neotectonics of southern Africa. Afr. Geosci. Rev. 3, 1–16.
Aslanian, D., Moulin, M., 2013. Palaeogeographic consequences of conservational models in the South Atlantic Ocean. Geol. Soc. Lond. Spec. Publ. 369 (1), 75–90.
Autin, J., Bellahsen, N., Leroy, S., Husson, L., Beslier, M.O., d'Acremont, E., 2013. The role of structural inheritance in oblique rifting: insights from analogue models and application to the Gulf of Aden. Tectonophysics 607, 51–64.
Ballard, S., Pollack, H.N., 1987. Diversion of heat by Archean cratons: a model for southern Africa. Earth Planet. Sci. Lett. 85 (1), 253–264.
Basson, I.J., Viola, G., 2004. Passive kimberlite intrusion into actively dilating dyke fracture arrays: evidence from fibrous calcite veins and extensional fracture cleavage. Lithos 76 (1), 283–297.
Bate, K.J., Malan, J.A., 1992. Tectonostratigraphic evolution of the Algoa, Gamtoos and Pletmos basins, offshore South Africa. Inversion Tectonics of the Cape Fold Belt. Karoo and Cretaceous Basins of Southern Africa, Rotterdam, Balkema, pp. 61–73.
Ben-Avraham, Z., Hartnady, C.J.H., Malan, J.A., 1993. Early tectonic extension between the Agulhas Bank and the Falkland Plateau due to the rotation of the Lafonia microplate. Earth Planet. Sci. Lett. 117 (1), 43–58.
Ben-Avraham, Z., Hartnady, C.J.H., Le Roex, A.P., 1995. Neotectonic activity on continental fragments in the southwest Indian Ocean: Agulhas Plateau and Mozambique Ridge. J. Geophys. Res. Solid Earth (1978–2012) 100 (B4), 6199–6211.
Ben-Avraham, Z., Hartnady, C.J.H., Kitchin, K.A., 1997. Structure and tectonics of the Agulhas–Falkland fracture zone. Tectonophysics 282 (1), 83–98.
Bird, P., Ben-Avraham, Z., Schubert, G., Andreoli, M., Viola, G., 2006. Patterns of stress and strain rate in southern Africa. J. Geophys. Res. Solid Earth (1978–2012) 111 (B8).
Blenkinsop, T., Moore, A., 2013. Tectonic geomorphology of passive margins and continental hinterlands. In: Owen, L.A. (Ed.), Treatise on Geomorphology. Tectonic Geomorphology vol. 5. Academic Press, San Diego, CA, pp. 71–92.
Boyd, D., Anka, Z., Di Primio, R., Kuhlmann, G., De Wit, M.J., 2011. Passive margin evolution and controls on natural gas leakage in the Orange Basin, South Africa. S. Afr. J. Geol. 114 (3-4), 415–432.
Brandt, D., Andreoli, M.A.G., McCarthy, T.S., 2003. Mesozoic fluvial deposits on a rifted continental margin near Vaalputs, Namaqualand, South Africa. S. Afr. J. Geol. 106 (1), 11–16.
Brandt, D., Andreoli, M.A.G., McCarthy, T.S., 2005. The late Mesozoic palaeosoils and Cenozoic fluvial deposits at Vaalputs, Namaqualand, South Africa: possible depositional mechanisms and their bearing on the evolution of the continental margin. S. Afr. J. Geol. 108 (2), 271–284.
Braun, J., Beaumont, C., 1989. A physical explanation of the relation between flank uplifts and the breakup unconformity at rifted continental margins. Geology 17 (8), 760–764.
Braun, J., Robert, Xavier, Simon-Labric, T., 2013. Eroding dynamic topography. Geophys. Res. Lett. 40, 1494–1499.
Broad, D.S., Jungslager, E.H.A., McLachlan, I.R., Roux, J., van der Spuy, D., 2012. South Africa's Mesozoic offshore basins. In: Roberts, D.G., Bally, A.W. (Eds.), Regional

Geology and Tectonics: Phanerozoic Passive Margins. Cratonic Basins and Global Tectonic Maps: Phanerozoic Passive Margins, Cratonic Basins and Global Tectonic Maps vol. 1C. Elsevier, pp. 535–564.
Brown, R.W., Rust, D.J., Summerfield, M.A., Gleadow, A.J., de Wit, M.C., 1990. An Early Cretaceous phase of accelerated erosion on the south-western margin of Africa: evidence from apatite fission track analysis and the offshore sedimentary record. Int. J. Radiat. Appl. Instrum. Part D 17 (3), 339–350.
Brown, R.W., Summerfield, M.A., Gleadow, A.J., 1994. Apatite fission track analysis: its potential for the estimation of denudation rates and implications for models of long-term landscape development. Process Models and Theoretical Geomorphologypp. 24–53.
Brown, L.F., Brink, G.J., Benson, J.M., 1995. Sequence Stratigraphy in Offshore South African Divergent Basins: An Atlas on Exploration for Cretaceous Lowstand Traps by Soekor (Pty) Ltd. American Association of Petroleum Geologists.
Brown, R.W., Gallagher, K., Gleadow, A.J., Summerfield, M.A., 2000. Morphotectonic evolution of the South Atlantic margins of Africa and South America. In: Summerfield, M.A. (Ed.), Geomorphology and Global Tectonics. Wiley, Chichester, pp. 255–281.
Brown, R.W., Summerfield, M.A., Gleadow, A.J., 2002. Denudational history along a transect across the Drakensberg Escarpment of southern Africa derived from apatite fission track thermochronology. J. Geophys. Res. 107 (B12), 2350.
Brown, R., Summerfield, M., Gleadow, A., Gallagher, K., Carter, A., Beucher, R., Wildman, M., 2014. Intracontinental deformation in southern Africa during the Late Cretaceous. J. Afr. Earth Sci. 100, 20–41.
Brune, S., Heine, C., Pérez-Gussinyé, M., Sobolev, S.V., 2014. Rift migration explains continental margin asymmetry and crustal hyper-extension. Nat. Commun. 5, 1–9.
Bumby, A.J., Guiraud, R., 2005. The geodynamic setting of the Phanerozoic basins of Africa. J. Afr. Earth Sci. 43 (1), 1–12.
Burke, K., Gunnell, Y., 2008. The African erosion surface: a continental-scale synthesis of geomorphology, tectonics, and environmental change over the past 180 million years. Geol. Soc. Am. Mem. 201, 66.
Cande, S.C., Stegman, D.R., 2011. Indian and African plate motions driven by the push force of the Reunion plume head. Nature 475 (7354), 47–52.
Cande, S.C., LaBrecque, J.L., Haxby, W.F., 1988. Plate kinematics of the South Atlantic: chron C34 to present. J. Geophys. Res. Solid Earth (1978–2012) 93 (B11), 13479–13492.
Carlson, W.D., Donelick, R.A., Ketcham, R.A., 1999. Variability of apatite fission-track annealing kinetics: I. Experimental results. Am. Mineral. 84, 1213–1223.
Cateneanu, O., Wopfner, H., Eriksson, P.G., Cairncross, B., Rubidge, B.S., Smith, R.M.H., Hancox, P.J., 2005. The Karoo basins of south-central Africa. J. Afr. Earth Sci. 43 (1), 211–253.
Cockburn, H.A.P., Brown, R.W., Summerfield, M.A., Seidl, M.A., 2000. Quantifying passive margin denudation and landscape development using a combined fission-track thermochronology and cosmogenic isotope analysis approach. Earth Planet. Sci. Lett. 179 (3), 429–435.
Cogné, N., Gallagher, K., Cobbold, P.R., 2011. Post-rift reactivation of the onshore margin of southeast Brazil: evidence from apatite (U–Th)/He and fission-track data. Earth Planet. Sci. Lett. 309 (1), 118–130.
Cornelissen, A.K., Verwoerd, W.J., 1975. The Bushmanland kimberlites and related rocks. Phys. Chem. Earth 9, 71–80.
Cornell, D.H., Thomas, R.J., Gibson, R., Moen, H.F.G., Reid, D.L., Moore, J.M., Gibson, R.L., 2006. The Namaqua-Natal Province. Geol. Soc. S. Afr. 325–379.
Corti, G., Ranalli, G., Agostini, A., Sokoutis, D., 2013. Inward migration of faulting during continental rifting: effects of pre-existing lithospheric structure and extension rate. Tectonophysics 594, 137–148.
Courtillot, V., Jaupart, C., Manighetti, I., Tapponnier, P., Besse, J., 1999. On causal links between flood basalts and continental breakup. Earth Planet. Sci. Lett. 166 (3), 177–195.
Cox, K.G., 1992. Karoo igneous activity, and the early stages of the break-up of Gondwanaland. Geol. Soc. Lond. Spec. Publ. 68 (1), 137–148.
Curtis, C.G., Trumbull, R.B., de Beer, C.H., Harris, C., Reid, D.L., Romer, R.L., 2011. Geochemistry of the early Cretaceous Koegel Fontein anorogenic igneous complex, South Africa. S. Afr. J. Geol. 114 (3-4), 353–378.
Daly, M.C., Chorowicz, J., Fairhead, J.D., 1989. Rift basin evolution in Africa: the influence of reactivated steep basement shear zones. Geol. Soc. Lond. Spec. Publ. 44 (1), 309–334.
Dauteuil, O., Bessin, P., Guillocheau, F., 2014. Topographic growth around the Orange River valley, southern Africa: A Cenozoic record of crustal deformation and climatic change. Geomorphology 233, 5–19.
Day, R.W., 1987. False Bay dolerites. Ann. Geol. Surv. S. Afr. 21, 1–7.
de Beer, C.H., 2012. Evidence of Neogene to Quaternary faulting and seismogenic deformation along the Namaqualand coast, South Africa. S. Afr. J. Geol. 115 (2), 117–136.
de Vera, J., Granado, P., McClay, K., 2010. Structural evolution of the Orange Basin gravity-driven system, offshore Namibia. Mar. Pet. Geol. 27 (1), 223–237.
de Wit, M.C.J., 1988. Aspects of the geomorphology of the north-western Cape, South Africa. Geomorphological Studies in Southern Africa. Balkema, Rotterdam, The Netherlands, pp. 57–69.
de Wit, M.C.J., 1999. Post-Gondwana drainage and the development of diamond placers in western South Africa. Econ. Geol. 94 (5), 721–740.
de Wit, M.J., Ransome, I.G., 1992. Regional inversion tectonics along the southern margin of Gondwana. Inversion Tectonics of the Cape Fold Belt, Karoo and Cretaceous Basins of Southern Africa. Balkema, Rotterdam, pp. 15–21.
de Wit, M.C.J., Ward, J.D., Spaggiari, R., 1992. A reappraisal of the Kangnas dinosaur site, Bushmanland, South Africa. S. Afr. J. Sci. 88 (9-10), 504–507.
Decker, J.E., Niedermann, S., de Wit, M.J., 2013. Climatically influenced denudation rates of the southern African plateau: clues to solving a geomorphic paradox. Geomorphology 190, 48–60.
Delvaux, D., 2001. Karoo rifting in western Tanzania: precursor of Gondwana breakup. Contributions to Geology and Paleontology of Gondwana in Honor of Helmut Wopfner. Geological Institute, University of Cologne, Cologne, pp. 111–125.
Dewey, J.F., Robb, L., Van Schalkwyk, L., 2006. Did Bushmanland extensionally unroof Namaqualand? Precambrian Res. 150 (3), 173–182.
Dingle, R.V., 1982. Continental margin subsidence: a comparison between the east and west coasts of Africa. Dyn. Passive Margins 6, 59.
Dingle, R.V., Hendry, Q.B., 1984. Late Mesozoic and Tertiary sediment supply to the eastern Cape Basin (SE Atlantic) and palaeo-drainage systems in southwestern Africa. Mar. Geol. 56 (1), 13–26.
Dingle, R.V., Robson, S.H., 1992. Southwestern Africa continental rise: structural and sedimentary evolution. Geologic Evolution of Atlantic Continental Rises. Van Nostrand Reinhold, New York, pp. 62–76.
Dingle, R.V., Siesser, W.G., Newton, A.R., 1983. Mesozoic and Tertiary Geology of Southern Africa. A. A. Balkema, Rotterdam (375 pp.).
Donelick, R.A., Ketcham, R.A., Carlson, W.D., 1999. Variability of apatite fission-track annealing kinetics: II. Crystallographic orientation effects. American Mineralogist 84, 1224–1234.
Donelick, R.A., O'Sullivan, P.B., Ketcham, R.A., 2005. Apatite fission-track analysis. Rev. Mineral. Geochem. 58 (1), 49–94.
Duncan, R.A., Hooper, P.R., Rehacek, J., Marsh, J.S., Duncan, A.R., 1997. The timing and duration of the Karoo igneous event, southern Gondwana. J. Geophys. Res. 102, 18127–18138.
Eagles, G., 2007. New angles on South Atlantic opening. Geophys. J. Int. 168 (1), 353–361.
Eglington, B.M., 2006. Evolution of the Namaqua–Natal Belt, southern Africa—a geochronological and isotope geochemical review. J. Afr. Earth Sci. 46 (1), 93–111.
Elburg, M., Goldberg, A., 2000. Age and geochemistry of Karoo dolerite dykes from north-east Botswana. J. Afr. Earth Sci. 31 (3), 539–554.
Fairhead, J.D., 1988. Mesozoic and Cenozoic plate tectonic reconstructions of the central South Atlantic Ocean: the role of the West and Central African Rift System. Tectonophysics 155, 181–191.
Flowers, R.M., Schoene, B., 2010. (U–Th)/He thermochronometry constraints on unroofing of the eastern Kaapvaal craton and significance for uplift of the southern African Plateau. Geology 38 (9), 827–830.
Forte, A.M., Quéré, S., Moucha, R., Simmons, N.A., Grand, S.P., Mitrovica, J.X., Rowley, D.B., 2010. Joint seismic–geodynamic-mineral physical modelling of African geodynamics: a reconciliation of deep-mantle convection with surface geophysical constraints. Earth Planet. Sci. Lett. 295 (3), 329–341.
Foster, D.A., Gleadow, A.J., 1992. Reactivated tectonic boundaries and implications for the reconstruction of southeastern Australia and northern Victoria Land, Antarctica. Geology 20 (3), 267–270.
Frimmel, H.E., 2000. The Pan-African Gariep Belt in southwestern Namibia and western South Africa. Commun. Geol. Surv. Namibia 12, 197–209.
Frimmel, H.E., Fölling, P.G., Diamond, R., 2001. Metamorphism of the Permo-Triassic Cape Fold Belt and its basement, South Africa. Mineral. Petrol. 73 (4), 325–346.
Gaina, C., Torsvik, T.H., van Hinsbergen, D.J., Medvedev, S., Werner, S.C., Labails, C., 2013. The African Plate: a history of oceanic crust accretion and subduction since the Jurassic. Tectonophysics 604, 4–25.
Gallagher, K., 2012. Transdimensional inverse thermal history modeling for quantitative thermochronology. J. Geophys. Res. Solid Earth (1978–2012) 117 (B2).
Gallagher, K., Brown, R., Johnson, C., 1998. Fission track analysis and its applications to geological problems. Annu. Rev. Earth Planet. Sci. 26 (1), 519–572.
Gallagher, K., Charvin, K., Nielsen, S., Sambridge, M., Stephenson, J., 2009. Markov chain Monte Carlo (MCMC) sampling methods to determine optimal models, model resolution and model choice for Earth Science problems. Mar. Pet. Geol. 26 (4), 525–535.
Garver, J.I., Reiners, P.W., Walker, L.J., Ramage, J.M., Perry, S.E., 2005. Implications for timing of Andean uplift from thermal resetting of radiation-damaged zircon in the Cordillera Huayhuash, Northern Peru. J. Geol. 113 (2), 117–138.
Gerrard, I., Smith, G.C., 1982. Post-Paleozoic succession and structure of the southwestern African continental margin. Studies in continental margin geology. AAPG Mem. 34, 49–74.
Gibson, G.M., Totterdell, J.M., White, L.T., Mitchell, C.H., Stacey, A.R., Morse, M.P., Whitaker, A., 2013. Pre-existing basement structure and its influence on continental rifting and fracture zone development along Australia's southern rifted margin. J. Geol. Soc. 170 (2), 365–377.
Gilchrist, A.R., Summerfield, M.A., 1991. Denudation, isostasy and landscape evolution. Earth Surf. Process. Landf. 16 (6), 555–562.
Gilchrist, A.R., Kooi, H., Beaumont, C., 1994. Post-Gondwana geomorphic evolution of southwestern Africa: implications for the controls on landscape development from observations and numerical experiments. J. Geophys. Res. Solid Earth (1978–2012) 99 (B6), 12211–12228.
Gilks, W.R., 2005. Markov Chain Monte Carlo. John Wiley & Sons, Ltd.
Gombosi, D.J., Garver, J.I., Baldwin, S.L., 2014. On the development of electron microprobe zircon fission-track geochronology. Chem. Geol. 363, 312–321.
Goodlad, S.W., Martin, A.K., Hartnady, C.J.H., 1982. Mesozoic magnetic anomalies in the southern Natal Valley. Nature 295 (5851), 686–688.
Gough, D.I., 1963. Heat flow in the Southern Karroo. Proc. R. Soc. Lond. Ser. A Math. Phys. Sci. 272 (1349), 207–230.
Green, R.W.E., Bloch, S., 1971. The Ceres, South Africa, earthquake of September 29, 1969 I. Report on some aftershocks. Bull. Seismol. Soc. Am. 61 (4), 851–859.
Green, P.F., Lidmar-Bergström, K., Japsen, P., Bonow, J.M., Chalmers, J.A., 2013. Stratigraphic landscape analysis, thermochronology and the episodic development of elevated, passive continental margins. Geol. Surv. Den. Greenl. Bull. 30, 1–150.
Gresse, P.G., Theron, J.N., Fitch, F.J., Miller, J.A., 1992. Tectonic inversion and radiometric resetting of the basement in the Cape Fold Belt. Inversion Tectonics of the Cape

Fold Belt, Karoo and Cretaceous Basins of Southern Africa. Balkema, Rotterdam, pp. 217–228.
Gresse, P.G., Von Veh, M.W., Frimmel, H.E., 2006. Namibian (Neoproterozoic) to early Cambrian successions. The Geology of South Africa. Geological Society of South Africa, Johannesburg, pp. 395–420.
Groenewald, P.B., Grantham, G.H., Watkeys, M.K., 1991. Geological evidence for a Proterozoic to Mesozoic link between southeastern Africa and Dronning Maud Land, Antarctica. J. Geol. Soc. 148 (6), 1115–1123.
Guillocheau, F., Rouby, D., Robin, C., Helm, C., Rolland, N., Le Carlier De Veslud, C., Braun, J., 2012. Quantification and causes of the terrigeneous sediment budget at the scale of a continental margin: a new method applied to the Namibia–South Africa margin. Basin Res. 24 (1), 3–30.
Gunnell, Y., Gallagher, K., Carter, A., Widdowson, M., Hurford, A.J., 2003. Denudation history of the continental margin of western peninsular India since the early Mesozoic—reconciling apatite fission-track data with geomorphology. Earth Planet. Sci. Lett. 215 (1), 187–201.
Gurnis, M., Mitrovica, J.X., Ritsema, J., Van Heijst, H.J., 2000. Constraining mantle density structure using geological evidence of surface uplift rates: the case of the African Superplume. Geochem. Geophys. Geosyst. 1 (7), 1020–1031.
Haddon, I.G., McCarthy, T.S., 2005. The Mesozoic–Cenozoic interior sag basins of Central Africa: the Late-Cretaceous–Cenozoic Kalahari and Okavango basins. J. Afr. Earth Sci. 43 (1), 316–333.
Hälbich, I.W., 1993. Cape Fold Belt-Agulhas bank transect across Gondwana suture, Southern Africa. American Geophysical Union vol. 9 pp. 1–20.
Hälbich, I.W., Fitch, F.J., Miller, J.A., 1983. Geodynamics of the Cape Fold Belt, Special Publication, No. 12. Geological Society of South Africa, Johannesburg (South Africa) (191 pp.).
Hartnady, C.J.H., Newton, A.R., Theron, J.N., 1974. The stratigraphy and structure of the Malmesbury Group in the southwestern Cape. Bull. Precambrian Res. Unit 15, 193–213.
Hartwig, A., di Primio, R., Anka, Z., Horsfield, B., 2012. Source rock characteristics and compositional kinetic models of Cretaceous organic rich black shales offshore southwestern Africa. Org. Geochem. 51, 17–34.
Haughton, S.H., 1931. The late Tertiary and Recent deposits of the west coast of South Africa. Trans. Geol. Soc. S. Afr. 34, 19–57.
Hawkesworth, C.J., Gallagher, K., Kirstein, L., Mantovani, M.S.M., Peate, D.W., Turner, S.P., 2000. Tectonic controls on magmatism associated with continental breakup: an example from the Paraná–Etendeka Province. Earth Planet. Sci. Lett. 179 (2), 335–349.
Hirsch, K.K., Bauer, K., Scheck-Wenderoth, M., 2009. Deep structure of the western South African passive margin—results of a combined approach of seismic, gravity and isostatic investigations. Tectonophysics 470 (1), 57–70.
Hirsch, K.K., Scheck-Wenderoth, M., van Wees, J.D., Kuhlmann, G., Paton, D.A., 2010. Tectonic subsidence history and thermal evolution of the Orange Basin. Mar. Pet. Geol. 27 (3), 565–584.
Huismans, R.S., Beaumont, C., 2008. Complex rifted continental margins explained by dynamical models of depth-dependent lithospheric extension. Geology 36 (2), 163–166.
Huismans, R., Beaumont, C., 2011. Depth-dependent extension, two-stage breakup and cratonic underplating at rifted margins. Nature 473 (7345), 74–78.
Japsen, P., Bonow, J.M., Green, P.F., Chalmers, J.A., Lidmar-Bergström, K., 2006. Elevated, passive continental margins: long-term highs or Neogene uplifts? New evidence from West Greenland. Earth Planet. Sci. Lett. 248 (1), 330–339.
Japsen, P., Chalmers, J.A., Green, P.F., Bonow, J.M., 2012. Elevated, passive continental margins: not rift shoulders, but expressions of episodic, post-rift burial and exhumation. Glob. Planet. Chang. 90, 73–86.
Jelsma, H., Barnett, W., Richards, S., Lister, G., 2009. Tectonic setting of kimberlites. Lithos 112, 155–165.
John, B.E., Foster, D.A., 1993. Structural and thermal constraints on the initiation angle of detachment faulting in the southern Basin and Range: the Chemehuevi Mountains case study. Geol. Soc. Am. Bull. 105 (8), 1091–1108.
Jokat, W., Boebel, T., König, M., Meyer, U., 2003. Timing and geometry of early Gondwana breakup. J. Geophys. Res. Solid Earth (1978–2012) 108 (B9).
Jones, M.Q.W., 1987. Heat flow and heat production in the Namaqua mobile belt, South Africa. J. Geophys. Res. 92 (B7), 6273–6289.
Jourdan, F., Féraud, G., Bertrand, H., Kampunzu, A.B., Tshoso, G., Le Gall, B., Tiercelin, J.J., Capiez, P., 2004. The Karoo triple junction questioned: evidence from Jurassic and Proterozoic $^{40}Ar/^{39}Ar$ ages and geochemistry of the giant Okavango dyke swarm (Botswana). Earth Planet. Sci. Lett. 222 (3), 989–1006.
Jourdan, F., Féraud, G., Bertrand, H., Kampunzu, A.B., Tshoso, G., Watkeys, M.K., Le Gall, B., 2005. Karoo large igneous province: brevity, origin, and relation to mass extinction questioned by new $^{40}Ar/^{39}Ar$ age data. Geology 33 (9), 745–748.
Jourdan, F., Féraud, G., Bertrand, H., Watkeys, M.K., Renne, P.R., 2007. Distinct brief major events in the Karoo large igneous province clarified by new $^{40}Ar/^{39}Ar$ ages on the Lesotho Basalts. Lithos 98 (1), 195–209.
Jungslager, E.H., 1999. Petroleum habitats of the Atlantic margin of South Africa. Geol. Soc. Lond. Spec. Publ. 153 (1), 153–168.
Kasuya, M., Naeser, C.W., 1988. The effect of α-damage on fission-track annealing in zircon. Int. J. Radiat. Appl. Instrum. Part D 14 (4), 477–480.
Ketcham, R.A., Carter, A., Donelick, R.A., Barbarand, J., Hurford, A.J., 2007. Improved modeling of fission-track annealing in apatite. Am. Mineral. 92 (5-6), 799–810.
König, M., Jokat, W., 2006. The Mesozoic breakup of the Weddell Sea. J. Geophys. Res. Solid Earth (1978–2012) 111 (B12).
König, M., Jokat, W., 2010. Advanced insights into magmatism and volcanism of the Mozambique Ridge and Mozambique Basin in the view of new potential field data. Geophys. J. Int. 180 (1), 158–180.
Kooi, H., Beaumont, C., 1994. Escarpment evolution on high-elevation rifted margins: insights derived from a surface processes model that combines diffusion, advection, and reaction. J. Geophys. Res. 99 (B6), 12191–12209.
Koopmann, H., Franke, D., Schreckenberger, B., Schulz, H., Hartwig, A., Stollhofen, H., di Primio, R., 2013. Segmentation and volcano-tectonic characteristics along the SW African continental margin, South Atlantic, as derived from multichannel seismic and potential field data. Mar. Pet. Geol. 50, 22–39.
Kounov, A., Niedermann, S., De Wit, M.J., Viola, G., Andreoli, M., Erzinger, J., 2007. Present denudation rates at selected sections of the South African escarpment and the elevated continental interior based on cosmogenic 3He and 21Ne. S. Afr. J. Geol. 110 (2-3), 235–248.
Kounov, A., Viola, G., De Wit, M., Andreoli, M.A.G., 2009. Denudation along the Atlantic passive margin: new insights from apatite fission-track analysis on the western coast of South Africa. Geol. Soc. Lond. Spec. Publ. 324 (1), 287–306.
Kovacs, L.C., Morris, P., Brozena, J., Tikku, A., 2002. Seafloor spreading in the Weddell Sea from magnetic and gravity data. Tectonophysics 347 (1), 43–64.
Kröner, A., 1977. The Precambrian geotectonic evolution of Africa: plate accretion versus plate destruction. Precambrian Res. 4 (2), 163–213.
Krüger, F., Scherbaum, F., 2014. The 29 September 1969, Ceres, South Africa, Earthquake: full waveform moment tensor inversion for point source and kinematic source parameters. Bull. Seismol. Soc. Am. 104. http://dx.doi.org/10.1785/0120130209.
Kuhlmann, G., Adams, S., Campher, C., van der Spuy, D., di Primio, R., Horsfield, B., 2010. Passive margin evolution and its controls on natural gas leakage in the southern Orange Basin, blocks 3/4, offshore South Africa. Mar. Pet. Geol. 27 (4), 973–992.
Laslett, G.M., Green, P.F., Duddy, I.R., Gleadow, A.J.W., 1987. Thermal annealing of fission tracks in apatite 2. A quantitative analysis. Chem. Geol. Isot. Geosci. Sect. 65 (1), 1–13.
Lindeque, A.S., Ryberg, T., Stankiewicz, J., Weber, M.H., De Wit, M.J., 2007. Deep crustal seismic reflection experiment across the southern Karoo Basin, South Africa. S. Afr. J. Geol. 110 (2-3), 419–438.
Lindeque, A., de Wit, M.J., Ryberg, T., Weber, M., Chevallier, L., 2011. Deep crustal profile across the southern Karoo Basin and Beattie Magnetic Anomaly, South Africa: an integrated interpretation with tectonic implications. S. Afr. J. Geol. 114 (3-4), 265–292.
Lisker, F., Ventura, B., Glasmacher, U.A., 2009. Apatite thermochronology in modern geology. Geol. Soc. Lond. Spec. Publ. 324 (1), 1–23.
Lithgow-Bertelloni, C., Silver, P.G., 1998. Dynamic topography, plate driving forces and the African superswell. Nature 395, 269–272.
Lock, B.E., Shone, R., Coates, A.T., Hatton, C.J., 1975. Mesozoic Newark type sedimentary basins within the Cape Fold belt of southern Africa. Proc. Int. Congr. Sedimentol., 9th, pp. 217–225.
Lundin, E.R., Doré, A.G., 2011. Hyperextension, serpentinization, and weakening: a new paradigm for rifted margin compressional deformation. Geology 39 (4), 347–350.
Marks, K.M., Tikku, A.A., 2001. Cretaceous reconstructions of East Antarctica, Africa and Madagascar. Earth Planet. Sci. Lett. 186 (3), 479–495.
Marsh, J.S., 1973. Relationships between transform directions and alkaline igneous rock lineaments in Africa and South America. Earth Planet. Sci. Lett. 18 (2), 317–323.
Marsh, J.S., Hooper, P.R., Rehacek, J.J., Duncan, R.A., Duncan, A.R., 1997. Stratigraphy and age of Karoo basalts of Lesotho and implications for correlations within the Karoo igneous province. Large Igneous Provinces: Continental, Oceanic, and Planetary Flood VolcanismAmerican Geophysical Union, Geophysical Monograph Series vol. 100 pp. 247–272.
Martin, A.K., Hartnady, C.J.H., 1986. Plate tectonic development of the South West Indian Ocean: a revised reconstruction of East Antarctica and Africa. J. Geophys. Res. Solid Earth (1978–2012) 91 (B5), 4767–4786.
Martin, A.K., Goodlad, S.W., Hartnady, C.J.H., Du Plessis, A., 1982. Cretaceous palaeopositions of the Falkland Plateau relative to southern Africa using Mesozoic seafloor spreading anomalies. Geophys. J. Int. 71 (3), 567–579.
Matmon, A., Bierman, P., Enzel, Y., 2002. Pattern and tempo of great escarpment erosion. Geology 30 (12), 1135–1138.
Maystrenko, Y.P., Scheck-Wenderoth, M., Hartwig, A., Anka, Z., Watts, A.B., Hirsch, K.K., Fishwick, S., 2013. Structural features of the Southwest African continental margin according to results of lithosphere-scale 3D gravity and thermal modelling. Tectonophysics 604, 104–121.
McMillan, I.K., 2003. Foraminiferally defined biostratigraphic episodes and sedimentation pattern of the Cretaceous drift succession (Early Barremian to Late Maastrichtian) in seven basins on the South African and southern Namibian continental margin. S. Afr. J. Sci. 99 (11 & 12), 537.
Menzies, M.A., Gallagher, K., Hurford, A.J., Yelland, A., 1997. Red Sea and Gulf of Aden rifted margins, Yemen: denudational histories and margin evolution. Geochim. Cosmochim. Acta 61, 2511–2527.
Milner, S.C., Le Roex, A.P., Watkins, R.T., 1993. Rb–Sr age determinations of rocks from the Okenyenya igneous complex, northwestern Namibia. Geol. Mag. 130 (03), 335–343.
Moore, A.E., 1976. Controls of post-Gondwanaland alkaline volcanism in southern Africa. Earth Planet. Sci. Lett. 31 (2), 291–296.
Moore, A.E., Verwoerd, W.J., 1985. The olivine melilitite–"kimberlite"–carbonatite suite of Namaqualand and Bushmanland, South Africa. S. Afr. J. Geol. 88 (2), 281–294.
Moore, A., Blenkinsop, T., Cotterill, F.W., 2008. Controls on post-Gondwana alkaline volcanism in Southern Africa. Earth Planet. Sci. Lett. 268 (1), 151–164.
Moore, A., Blenkinsop, T., Cotterill, F.W., 2009. Southern African topography and erosion history: plumes or plate tectonics? Terra Nova 21 (4), 310–315.
Moucha, R., Forte, A.M., 2011. Changes in African topography driven by mantle convection. Nat. Geosci. 4 (10), 707–712.
Moucha, R., Forte, A.M., Mitrovica, J.X., Rowley, D.B., Quéré, S., Simmons, N.A., Grand, S.P., 2008. Dynamic topography and long-term sea-level variations: there is no such thing as a stable continental platform. Earth Planet. Sci. Lett. 271 (1), 101–108.

Moulin, M., Fluteau, F., Courtillot, V., Marsh, J., Delpech, G., Quidelleur, X., Gérard, M., Jay, A.E., 2011. An attempt to constrain the age, duration, and eruptive history of the Karoo flood basalt: Naude's Nek section (South Africa). J. Geophys. Res. Solid Earth (1978–2012) 116 (B7).
Muntingh, A., Brown Jr., L.F., 1993. Sequence stratigraphy of petroleum plays, post-rift cretaceous rocks (Lower Aptian to Upper Maastrichtian). Orange Basin, Western Offshore, South Africa: Chapter 4: Recent Applications of Siliciclastic Sequence Stratigraphy.
Newton, A.R., Shone, R.W., Booth, P.W.K., 2006. The Cape fold belt. The Geology of South Africa. Geological Society of South Africa, Johannesburg, pp. 521–530.
Nürnberg, D., Müller, R.D., 1991. The tectonic evolution of the South Atlantic from Late Jurassic to present. Tectonophysics 191 (1), 27–53.
Nyblade, A.A., Robinson, S.W., 1994. The African superswell. Geophys. Res. Lett. 21 (9), 765–768.
Ollier, C.D., 1985. Morphotectonics of continental margins with great escarpments. In: Morisawa, M., Hack, J.T. (Eds.), Tectonic Geomorphology. Allen and Unwin, Boston, MA, pp. 3–25.
Ollier, C.D., Pain, C.F., 1997. Equating the basal unconformity with the palaeoplain: a model for passive margins. Geomorphology 19 (1), 1–15.
Parsiegla, N., Gohl, K., Uenzelmann-Neben, G., 2008. The Agulhas Plateau: structure and evolution of a large igneous province. Geophys. J. Int. 174 (1), 336–350.
Partridge, T.C., Maud, R.R., 1987. Geomorphic evolution of southern Africa since the Mesozoic. S. Afr. J. Geol. 90 (2), 179–208.
Partridge, T.C., Botha, G.A., Haddon, I.G., 2006. Cenozoic deposits of the interior. The Geology of South Africapp. 585–604.
Paton, D.A., 2006. Influence of crustal heterogeneity on normal fault dimensions and evolution: southern South Africa extensional system. J. Struct. Geol. 28 (5), 868–886.
Paton, D.A., Underhill, J.R., 2004. Role of crustal anisotropy in modifying the structural and sedimentological evolution of extensional basins: the Gamtoos Basin, South Africa. Basin Res. 16 (3), 339–359.
Paton, D.A., Macdonald, D.I., Underhill, J.R., 2006. Applicability of thin or thick skinned structural models in a region of multiple inversion episodes; southern South Africa. J. Struct. Geol. 28 (11), 1933–1947.
Paton, D.A., van der Spuy, D., di Primio, R., Horsfield, B., 2008. Tectonically induced adjustment of passive-margin accommodation space; influence on the hydrocarbon potential of the Orange Basin, South Africa. AAPG Bull. 92 (5), 589–609.
Paul, J.D., Roberts, G.G., White, N., 2014. The African landscape through space and time. Tectonics 33 (6), 898–935.
Peate, D.W., 1997. The Paraná–Etendeka Province. Large Igneous Provinces: Continental, Oceanic, and Planetary Flood Volcanismpp. 217–245.
Pedersen, V.K., Nielsen, S.B., Gallagher, K., 2012. The post-orogenic evolution of the Northeast Greenland Caledonides constrained from apatite fission track analysis and inverse geodynamic modelling. Tectonophysics 530, 318–330.
Raab, M.J., Brown, R.W., Gallagher, K., Carter, A., Weber, K., 2002. Late Cretaceous reactivation of major crustal shear zones in northern Namibia: constraints from apatite fission track analysis. Tectonophysics 349 (1), 75–92.
Raab, M.J., Brown, R.W., Gallagher, K., Weber, K., Gleadow, A.J.W., 2005. Denudational and thermal history of the Early Cretaceous Brandberg and Okenyenya igneous complexes on Namibia's Atlantic passive margin. Tectonics 24 (3).
Rahn, M.K., Brandon, M.T., Batt, G.E., Garver, J.I., 2004. A zero-damage model for fission-track annealing in zircon. Am. Mineral. 89 (4), 473–484.
Redfield, T.F., Osmundsen, P.T., Hendriks, B.W.H., 2005. The role of fault reactivation and growth in the uplift of western Fennoscandia. J. Geol. Soc. 162 (6), 1013–1030.
Reid, D.L., 1990. The Cape Peninsula dolerite dyke swarm, South Africa. Mafic Dikes and Emplacement Mechanisms. AA Balkema, Rotterdam, The Netherlands, pp. 325–334.
Reid, D.L., Rex, D.C., 1994. Cretaceous dykes associated with the opening of the South Atlantic; the Mehlberg Dyke, northern Richtersveld. S. Afr. J. Geol. 97 (2), 135–145.
Reid, D.L., Erlank, A.J., Rex, D.C., 1991. Age and correlation of the False Bay dolerite dyke swarm, south-western Cape, Cape Province. S. Afr. J. Geol. 94 (2-3), 155–158.
Richards, M.A., Duncan, R.A., Courtillot, V.E., 1989. Flood basalts and hot-spot tracks: plume heads and tails. Science 246 (4926), 103–107.
Ring, U., 1994. The influence of preexisting structure on the evolution of the Cenozoic Malawi rift (East African rift system). Tectonics 13 (2), 313–326.
Robb, L.J., Armstrong, R.A., Waters, D.J., 1999. The history of granulite-facies metamorphism and crustal growth from single zircon U–Pb geochronology: Namaqualand, South Africa. J. Petrol. 40 (12), 1747–1770.
Roberts, D.L., Botha, G.A., Maud, R.R., Pether, J., 2006. Coastal cenozoic deposits. The Geology of South Africa. Geological Society of South Africa, Johannesburg, pp. 605–628.
Rosendahl, B.R., 1987. Architecture of continental rifts with special reference to East Africa. Annu. Rev. Earth Planet. Sci. 15, 445.
Rouby, D., Bonnet, S., Guillocheau, F., Gallagher, K., Robin, C., Biancotto, F., Dauteuil, O., Braun, J., 2009. Sediment Supply to the Orange sedimentary system over the last 150 My: an evaluation from sedimentation/denudation balance. Mar. Pet. Geol. 26, 782–794.
Rouby, D., Braun, J., Robin, C., Dauteuil, O., Deschamps, F., 2013. Long-term stratigraphic evolution of Atlantic-type passive margins: a numerical approach of interactions between surface processes, flexural isostasy and 3D thermal subsidence. Tectonophysics 604, 83–103.
Rowsell, D.M., Connan, J., 1979. Oil generation, migration and preservation in the Middle Ecca sequence near Dannhauser and Wakkerstroom. Spec. Publ. Geol. Soc. S. Afr. 6, 131–150.
Salomon, E., Koehn, D., Passchier, C., Hackspacher, P.C., Glasmacher, U.A., 2014. Contrasting stress fields on correlating margins of the South Atlantic. Gondwana Research in press.
Sambridge, M., Gallagher, K., Jackson, A., Rickwood, P., 2006. Trans-dimensional inverse problems, model comparison and the evidence. Geophys. J. Int. 167 (2), 528–542.
Scheepers, R., Schoch, A.E., 2006. The Cape Granite Suite. The Geology of South Africa. Geological Society of South Africa, Johannesburg, pp. 421–432.
Schmitt, A.K., Emmermann, R., Trumbull, R.B., Bühn, B., Henjes-Kunst, F., 2000. Petrogenesis and $^{40}Ar/^{39}Ar$ geochronology of the Brandberg Complex, Namibia: evidence for a major mantle contribution in metaluminous and peralkaline granites. J. Petrol. 41 (8), 1207–1239.
Scholtz, A., 1985. The Palynology of the Upper Lacustrine Sediments of the Arnot Pipe, Banke, Namaqualand. vol. 95. The South African Museum.
Schumacher, M.E., 2002. Upper Rhine Graben: role of pre-existing structures during rift evolution. Tectonics 21 (1), 6-1.
Seward, D., Grujic, D., Schreurs, G., 2004. An insight into the breakup of Gondwana: identifying events through low-temperature thermochronology from the basement rocks of Madagascar. Tectonics 23 (3).
Smith, R.M.H., 1986. Sedimentation and palaeoenvironments of Late Cretaceous crater-lake deposits in Bushmanland, South Africa. Sedimentology 33 (3), 369–386.
Smith, C.B., Allsopp, H.L., Kramers, J.D., Hutchinson, G., Roddick, J.C., 1985. Emplacement ages of Jurassic-Cretaceous South African kimberlites by the Rb–Sr method on phlogopite and whole-rock samples. S. Afr. J. Geol. 88 (2), 249–266.
Sobel, E.R., Seward, D., 2010. Influence of etching conditions on apatite fission-track etch pit diameter. Chem. Geol. 271 (1), 59–69.
Sonibare, W.A., Sippel, J., Scheck-Wenderoth, M., Mikeš, D., 2015. Crust-scale 3D model of the Western Bredasdorp Basin (Southern South Africa): data-based insights from combined isostatic and 3D gravity modelling. Basin Res. 27 (2), 125–151.
Stanley, J.R., Flowers, R.M., Bell, D.R., 2013. Kimberlite (U–Th)/He dating links surface erosion with lithospheric heating, thinning, and metasomatism in the southern African Plateau. Geology 41 (12), 1243–1246.
Stump, E., 1992. The Ross Orogen of the Transantarctic Mountains in light of the Laurentia–Gondwana split. GSA Today 2 (2), 25–27.
Summerfield, M.A. (Ed.), 2000. Geomorphology and Global Tectonics. Wiley, Chichester.
Svensen, H., Corfu, F., Polteau, S., Hammer, Ø., Planke, S., 2012. Rapid magma emplacement in the Karoo large igneous province. Earth Planet. Sci. Lett. 325, 1–9.
Tagami, T., Shimada, C., 1996. Natural long-term annealing of the zircon fission track system around a granitic pluton. J. Geophys. Res. Solid Earth (1978–2012) 101 (B4), 8245–8255.
Tankard, A.J., Eriksson, S.C., Hunter, D.R., Jackson, M.P.A., Hobday, D.K., Minter, W.E.L., 1982. Crustal Evolution of Southern Africa: 3.8 Billion Years of Earth History. Springer-Verlag, New York, p. 523.
Tankard, A., Welsink, H., Aukes, P., Newton, R., Stettler, E., 2009. Tectonic evolution of the Cape and Karoo basins of South Africa. Mar. Pet. Geol. 26 (8), 1379–1412.
ten Brink, U., Stern, T., 1992. Rift flank uplifts and hinterland basins: comparison of the Transantarctic Mountains with the Great Escarpment of southern Africa. J. Geophys. Res. Solid Earth 97 (B1), 569–585.
Thomas, R.J., De Beer, C.H., Bowring, S.A., 1996. A comparative study of the Mesoproterozoic late orogenic porphyritic granitoids of southwest Namaqualand and Natal, South Africa. J. Afr. Earth Sci. 23 (3), 485–508.
Thomson, K., 1999. Role of continental break-up, mantle plume development and fault reactivation in the evolution of the Gamtoos Basin, South Africa. Mar. Pet. Geol. 16 (5), 409–429.
Tikku, A.A., Marks, K.M., Kovacs, L.C., 2002. An Early Cretaceous extinct spreading center in the northern Natal Valley. Tectonophysics 347 (1), 87–108.
Tinker, J., de Wit, M., Brown, R., 2008a. Mesozoic exhumation of the southern Cape, South Africa, quantified using apatite fission track thermochronology. Tectonophysics 455 (1), 77–93.
Tinker, J., de Wit, M., Brown, R., 2008b. Linking source and sink: evaluating the balance between onshore erosion and offshore sediment accumulation since Gondwana break-up, South Africa. Tectonophysics 455 (1), 94–103.
Tommasi, A., Vauchez, A., 2001. Continental rifting parallel to ancient collisional belts: an effect of the mechanical anisotropy of the lithospheric mantle. Earth Planet. Sci. Lett. 185 (1), 199–210.
Torsvik, T.H., Rousse, S., Labails, C., Smethurst, M.A., 2009. A new scheme for the opening of the South Atlantic Ocean and the dissection of an Aptian salt basin. Geophys. J. Int. 177 (3), 1315–1333.
Tremblay, A., Roden-Tice, M.K., Brandt, J.A., Megan, T.W., 2013. Mesozoic fault reactivation along the St. Lawrence rift system, eastern Canada: thermochronologic evidence from apatite fission-track dating. Geol. Soc. Am. Bull. 125 (5-6), 794–810.
Trueb, L., Ross, C.F., Smith, R., 2005. A new pipoid anuran from the Late Cretaceous of South Africa. J. Vertebr. Paleontol. 25 (3), 533–547.
Trumbull, R.B., Reid, D.L., de Beer, C., van Acken, D., Romer, R.L., 2007. Magmatism and continental breakup at the west margin of southern Africa: a geochemical comparison of dolerite dikes from northwestern Namibia and the Western Cape. S. Afr. J. Geol. 110 (2-3), 477–502.
Uenzelmann-Neben, G., Gohl, K., 2004. The Agulhas Ridge, South Atlantic: the peculiar structure of a fracture zone. Mar. Geophys. Res. 25 (3-4), 305–319.
Uenzelmann-Neben, G., Gohl, K., Ehrhardt, A., Seargent, M., 1999. Agulhas Plateau, SW Indian Ocean: new evidence for excessive volcanism. Geophys. Res. Lett. 26 (13), 1941–1944.
Unternehr, P., Curie, D., Olivet, J.L., Goslin, J., Beuzart, P., 1988. South Atlantic fits and intraplate boundaries in Africa and South America. Tectonophysics 155, 169–179.
van der Beek, P., Braun, J., 1998. Numerical modelling of landscape evolution on geological time-scales: a parameter analysis and comparison with the south-eastern highlands of Australia. Basin Res. 10 (1), 49–68.
van der Beek, P., Summerfield, M.A., Braun, J., Brown, R.W., Fleming, A., 2002. Modelling post breakup landscape development and denudational history across

the southeast African (Drakensberg Escarpment) margin. J. Geophys. Res. 107 (B12), 2351.
Van der Merwe, R., Fouche, J., 1992. Inversion tectonics in the Bredasdorp basin, offshore South Africa. Inversion Tectonics of the Cape Fold Belt, Karoo and Cretaceous Basins of Southern Africa. Balkema, Rotterdam, Netherlands, pp. 49–60.
Van der Spuy, D., 2003. Aptian source rocks in some South African Cretaceous basins. Geol. Soc. Lond. Spec. Publ. 207 (1), 185–202.
Verwoerd, W.J., de Beer, C.H., 2006. Cretaceous and Tertiary igneous events. The Geology of South Africapp. 573–583.
Viljoen, J.H.A., 1992. The stratigraphy of the Heidelberg/Riversdale Mesozoic Basin. Inversion Tectonics of the Cape Fold Belt, Karoo and Cretaceous Basins of Southern Africa. Balkema, Rotterdam, Netherlands, pp. 77–84.
Viola, G., Andreoli, M., Ben-Avraham, Z., Stengel, I., Reshef, M., 2005. Offshore mud volcanoes and onland faulting in southwestern Africa: Neotectonic implications and constraints on the regional stress field. Earth Planet. Sci. Lett. 231 (1), 147–160.
Viola, G., Kounov, A., Andreoli, M.A., Mattila, J., 2012. Brittle tectonic evolution along the western margin of South Africa: more than 500 Myr of continued reactivation. Tectonophysics 514, 93–114.
Watkins, R.T., McDougall, I., Le Roex, A.P., 1994. K–Ar ages of the Brandberg and Okenyenya igneous complexes, north-western Namibia. Active Continental Margins—Present and Past. Springer, Berlin Heidelberg, pp. 348–356.
White, R., McKenzie, D., 1989. Magmatism at rift zones: the generation of volcanic continental margins and flood basalts. J. Geophys. Res. Solid Earth (1978–2012) 94 (B6), 7685–7729.
White, S., Stollhofen, H., Stanistreet, I.G., Lorenz, V., 2009. Pleistocene to recent rejuvenation of the Hebron Fault, SW Namibia. Geol. Soc. Lond. Spec. Publ. 316 (1), 293–317.
Wigley, R.A., Compton, J.S., 2006. Late Cenozoic evolution of the outer continental shelf at the head of the Cape Canyon, South Africa. Mar. Geol. 226 (1), 1–23.
Yamada, R., Tagami, T., Nishimura, S., Ito, H., 1995. Annealing kinetics of fission tracks in zircon: an experimental study. Chem. Geol. 122 (1), 249–258.
Yamada, R., Murakami, M., Tagami, T., 2007. Statistical modelling of annealing kinetics of fission tracks in zircon; reassessment of laboratory experiments. Chem. Geol. 236 (1), 75–91.